Investigation of Exothermic Reaction Dynamics via Computational Fluid Dynamics Coupled with a Feedback Controller

by

SIUSAN CHOI

Presented to the Faculty of the Graduate School of
The University of Texas at Arlington in Partial Fulfillment
of the Requirements
for the Degree of

DOCTOR OF PHILOSOPHY

THE UNIVERSITY OF TEXAS AT ARLINGTON

July 2016

Acknowledgements

Most importantly, I would like to express my most sincere gratitude to my supervising professor, Dr. Brian H. Dennis, for his patience and guidance in supporting me during my PhD study. I am deeply appreciative of his mentorship and wise knowledge in helping me to accomplish my research; without his given assistance, the completion of this thesis would not have been possible. Furthermore, his guidance was not only useful during my PhD study but also I am confident it will prove beneficial along my future career path.

Next, I would like to give thanks to my committee members for their valuable time and comments regarding this thesis. Special thanks to Dr. Kamesh Subbarao for his knowledge and time in helping me successfully realize this thesis.

In addition, I would like to deeply thank my colleagues in the CFD lab and CREST lab for their advice and guidance: Dr. Rachaneewan Charoenwat, Dr. Wilaiwan Chanmanee, Dr. Alok A. Rege, and Pawarat Bootpakdeetam. Without their friendship and assistance, I would not have been able to complete this thesis.

Finally, I would like to thank my parents, Stephen Choi and Muiyee Wong, and my older sister, Shirley C. Hart, for their limitless support and encouragement throughout my life. Without their love, I would not have been raised in such a happy and healthy family.

Abstract

Investigation of Exothermic Reaction Dynamics via Computational Fluid Dynamics Coupled with a Feedback Controller

Siusan Choi, Ph.D.

The University of Texas at Arlington, 2016

Supervising Professor: Brian H. Dennis

The control of reaction temperature under continuous flow conditions is important in a variety of chemical manufacturing industries. For many reactions, operating at off-design temperatures can result in the production of undesired products, reduced feedstock conversion and, in some cases, reduced catalyst lifetime. In many exothermic reactions, maintaining a desired set point temperature at high reactant flow rates becomes challenging if the chemical kinetics exhibit highly non-linear behavior. In these situations, the interaction between commonly used linear controllers and the physical system can lead to unexpected dynamic response and undesired swings in reaction temperature.

In this research, a computational model was developed to investigate the effect of a linear feedback controller on exothermic reaction dynamics. A Proportional-Integral-Derivative Control (PID) controller was implemented in MATLAB and coupled with the computational fluid dynamics software FLUENT. The system was first tested with a simple heat source term with a user selectable non-linearity. The PID controller was found to work well for low energy densities,

but a steady oscillation in the reaction temperature was observed at high power densities where the non-linearity was large.

The software system was then used to study the interaction of a PID controller and a Fischer-Tropsch synthesis (FTS) reactor. Although many computational studies have been done for FTS, this is the first work to explore the effects of the controller on the dynamics of the model. A detailed kinetic model from the literature was used in FLUENT to simulate the FTS. Results for a steady-flow case were compared with published benchmark data to validate the FLUENT model. The coupled PID-FTS model was then run for different reactant flow rates and conditions similar to an experimental rig developed previously. The temperature response versus time at the center of the reactor was computed and compared with experiment data. At high flow rates, the computer model exhibited a temperature oscillation with a frequency close to that observed in the experiment. The results demonstrate that simulation can be used to replicate complex controller-chemical system interactions. This platform can be used in the future to test different control algorithms for FTS reactors before implementing them into the physical system and thus reduce the need to do numerous bench-top scale experiments in the laboratory.

TABLE OF CONTENTS

Page

LIST OF FIGURES

Page

LIST OF TABLES

Page

CHAPTER 1

INTRODUCTION

Petroleum is the main source of energy and provides over 40% of all the energy used in the world. As technology continues to advance, the consumption of petroleum has dramatically increased in every country. Many developing countries such as China and India, where the population is expected to soar in the future, have a high demand for petroleum as their economies continue to grow. With the global demand for petroleum higher than ever, there is the increasing danger of depleting reserves in the near future. The earth has only a limited amount of fossil fuel deposits, and the rate of harvesting them is much slower than their rate of consumption. Due to these factors, the price of petroleum has continuously increased. As the United States consumes the most amount of oil [1], the rise in the price of petroleum has caused a great impact on the economic and technological development in that country. Besides of the shortage, the environmental impacts of the combustion of petroleum are also well known. The carbon dioxide produced by combusting petroleum products is the main source of greenhouse gases, which contributes to increase the global warming effect. Therefore, reducing the demand for petroleum by developing an alternative fuel is critical to maintaining the high rate of science and technology contributions while minimizing the impact on the environment.

Many engineers and scientists have worked over the years searching for suitable alternative fuels to resolve this crisis, and many possible solutions have been explored. Out of all the possible solutions, natural gas may provide the best remedy to many of the aforementioned problems. Numerous studies have shown that natural gas produces up to 25% fewer emissions than burning

oil [2]. Furthermore, with advancements in drilling technology, more natural gas fields have been discovered domestically, which can supply a minimum of one hundred years of energy for North America [2]. Therefore, due the abundance of this alternative fuel, if it is efficiently exploited, energy prices will remain more stable and affordable for a long period of time.

Although natural gas has seemed to be the most promising fuel for the future, it has one major drawback. In many parts of the world, natural gas reserves are in remote locations, and several of them are even offshore. In addition, because it is a gas, the transportation is expensive and uneconomical [3]. However, with the use of the Fischer-Tropsch Synthesis process, the problem of transportation can be solved. The Fischer-Tropsch Synthesis (FTS) is a Gas-to-Liquid (GTL) process that can be used to convert the syngas reformed from natural gas into liquid hydrocarbons. In addition, because this process is well known, it could possibly be used at the natural gas reserve sites. This reduces the difficulty of transporting natural gas between desired locations.

1.1 History

Fischer-Tropsch Synthesis (FTS) is a Gas-to-Liquid (GTL) process named after the German scientists Franz Fischer and Hans Tropsch, who discovered the process in 1923 in order to satisfy the increased demand for fuel. FTS is a process that converts the gas mixture of carbon monoxide and hydrogen into liquid hydrocarbons through a series of catalytic chemical reactions. During the early part of 20^{th} century, many studies were conducted on GTL technology. In 1902, Sabatier and Senderens were the first to report that hydrocarbons could be catalytically synthesized from carbon monoxide and hydrogen using a nickel- or cobalt-based catalyst at atmospheric pressure [4]. Later in 1913, the Badische Anilin und Soda Fabrik (BASF) of Ludwigshafen, Germany applied for a patent for the “preparation of a liquid oil from synthesis gas” using cobalt and osmium based

catalysts [5]. However, the biggest breakthrough in the GTL process did not come until 1923, when Franz Fischer and Hans Tropsch of the Kaiser Wilhelm Institute for Coal Research (presently the Max Plank Institute) in Mülheim, Germany developed the FTS. Their process involved a reaction of carbon monoxide and hydrogen over an iron-based catalyst at a pressure of 150 atm and temperature of 400-450 ^{o}C [6]. They reported a resulting mixture of hydrocarbons. The resulting mixture was then fractionated by distillation and tested as a fuel on a 1922 model NSU motorbike. With better performance than the reference fuel, the success of the FTS process was marked [7].

During 1936, the first Fischer-Tropsch (FT) plant was built in Oberhausen, Germany with 52 reactors operating at atmospheric pressure and with a production capacity of 70,000 tons per year [8]. After the war, however, the demand for the fuel decreased, causing the FTS plants in Germany to cease operation. It was not until 1955 in South Africa that the first large-scale plant known as Sasol I was built and put into operation by the South African Coal, Oil and Gas Corporation's (SASOL) in Sasolburg [9]. Sasol I was operated using fixed-bed reactors and an iron base catalyst on silica as a support and copper as a promoter [10]. Later came two larger scale plants, Sasol II and Sasol III, in 1980 and 1982, but both plants were operated with syngas derived from coal instead of natural gas [9].

Despite the long history of the FTS technology, in recent years, many energy research groups have renewed interest in the FTS due to the rising price of oil and the discovery of large gas reserves. Certain aspects of the FTS process are still being studied. For example, the yield of products from the FTS depend on the catalyst and the process variables, including system temperature, space velocity, CO/H_2 gas feed ratio, and pressure. When these process variables are optimized and properly maintained, the yield products can be targeted to specific needs, for

example, the different octane numbers of gasoline. Compared to the products obtained from crude oil, FTS products require little to no refinery processing to reach a desired product, for example, car or plane fuel. In addition, Miroliaei et al. [11] showed that fuel produced from the FTS had a higher quality than the fuel obtained from other sources due to its very low aromaticity and the absence of sulfur. All of these advantages have made the FTS a very promising topic for research.

1.2 Background

This section discusses the development of the FTS process, including the different reactor designs, the selection of catalysts, and the studies on the reactor's computer model.

1.2.1 Reactor Design

The FT reaction is a well-known highly exothermic process; the average heat released during the process is about 145 kJ/mol [12], which is an order of magnitude higher than the typical oil refinery process. Moreover, the FTS process is highly sensitive to temperature. An increase in temperature not only causes an undesirable shift in the FT product selectivity but also results in deposition of the carbon on the catalyst and sintering of the material deposited on the catalyst. This in turn results in the deactivation of the catalyst and a reduction in the production rate of the FT process. Therefore, it is important for the reactor used in the FTS process to have the ability to rapidly transfer the heat from the catalyst to the reactor surface in order to maintain the catalyst bed in a near-isothermal condition. Three major FT reactor types have been studied during the long history of FTS development: the fixed-bed reactor, slurry bed reactor, and fluidized bed reactor. Much research has been done regarding these different reactor designs for the FTS process.

Fixed-bed reactor

The fixed-bed reactor is constructed with a fixed amount of catalyst placed in the reactor. Reactant gas enters through the inlet, reacts with the catalyst, and the products and excess gas leave through the outlet. The fixed-bed reactor system usually uses a narrow tube packed with small particles and operates at a high gas velocity in order to increase the heat exchange rate between the catalyst bed and the reactor surface. However, the combination of the narrow diameter tube, small particles, and high gas velocity results in an unacceptable increase in differential pressure occurring in the system [12]. An increase in differential pressure within the reactor can cause the disintegration of the catalyst and create a blockage in the reactor, increasing the overall maintenance cost of the system. Furthermore, the change in the pressure within the reactor also creates a change in operating condition, thereby resulting in a shift in the product selectivity of the FTS process. For these reasons, the design of the fixed-bed reactor has to make a compromise between the diameter of the reactor, the size of the catalyst particle, and the velocity of the gas.

Schulz et al. [13] placed the catalyst particles in a cylindrical vertical reactor with a reflux condenser fitted at the top, and liquid products were removed from the bottom. Ruhrchemie used a vertical slurry tube reactor that was inside a larger tube where oil circulated to remove heat from the system, and he used a reflux condenser to return heavy oil to the reactor [14]. Ruhrchemie also developed a device that sprayed oil on a fixed bed of catalysts to keep the catalysts free of wax and remove the heat from the reaction [15]. During the 1950s, Sasolburg designed a multi-tubular reactor to create heavy oil products, and their reactor operated very well [14]. In 1998, Sie proposed a fixed bed reactor that had a small amount of pressure drop inside the tube and a highly efficient heat removal capability [16].

Slurry bed reactor

During the 1950s and 60s, slurry-bed reactors were studied in many countries including Germany, England, and the United States. In all of these studies, however, the operating gas velocities were too low to be considered for practical interest. In principle, the slurry bed reactor should be best for a low temperature FT process that produces wax [12] because this reactor design can provide a longer retention time for the reactant gas and the catalyst to react. Furthermore, the capacity of this reactor is also the largest compared with the other two designs. Therefore, a more practical and efficient method of separating the wax from the catalyst is essential for this reactor to operate at its full potential.

Kölbel [17] developed the largest laboratory scale slurry phase reactor, but since the flow rate used was very low, the performance could not be judged [18]. Years later, ExxonMobil developed a slurry bed reactor operating with a Co-based catalyst and had successful demonstration runs [19]. Michael [20] also developed a laboratory scale reactor designed with an internal central tube fitted along its axis to cause rapid circulation of the slurry within.

Fluidized bed reactor

The fluidized bed reactor is by far the most complicated reactor design among all of the reactor types, yet it has the highest production rate. This reactor is designed so that the catalyst in the reaction section is swept up by the feeding gas from the bottom; the product gases then exit the reactor from the top. Since the bed is fluidized, the voidage in the reactor is large, which can increase the heat removal rate [12]. Hence, a highly isothermal condition can be achieved with this design. However, this design has its drawbacks. Beyond its more complicated design requiring higher capital costs, the fluidized bed system also presents a problem with catalyst poisoning.

Product gases like H_2S in the syngas can cause the catalyst to deactivate and therefore disable the system [12].

In the 1950s, Sasolburg Plant installed a fluidized-bed reactor designed by Kellogg [12]. It operated with an iron based catalyst at 340 °C and 2 MPa. Because the reactor had a fluidized bed and a large reaction chamber, the system reached a heat removal rate of 40%. The reactor was also designed with a recycle system to reuse the excess syngas from the outlet. Due to all of these factors, the conversion of the system reached approximately 90%. However, low capacity reactor was later replaced with a higher capacity reactor. In addition, a fluidized bed reactor was also installed in a plant in Brownsville, TX, but was later decommissioned due to the system's low conversion rate [12]. The plant reported that the system displayed a poor catalyst fluidization, causing the conversion rate to decrease and finally shutting the plant down.

1.2.2 Catalysts

In addition, the selection of catalysts greatly affects the result of the FTS process. Only four metals that belong to the Group VIII in the periodic table have activity sufficiently high for the hydrogenation of carbon monoxide and can be effectively used as catalysts for FTS: iron (Fe), cobalt (Co), nickel (Ni), and ruthenium (Ru) [12].

Of these four metals, Ru has shown the best performance as a catalyst for the FTS process due to its high activity. However, Ru-based catalyst has some weaknesses associated with it. Firstly, Ru is significantly more expensive than the other metals. Secondly, because of its high activity rate, the thermal control of the system with Ru as a catalyst would be difficult. Ni is also a highly active metal, but it is a powerful catalyst only for producing low hydrocarbon products like methane (CH_4) [12].

The most common metals to use for FT catalyst are Fe and Co. Fe is the cheaper material compared with the other three metals, and it has a high selectivity for heavy hydrocarbon products like wax. However, Fe-based catalysts also induce a powerful side reaction called the water gas shift (WGS) reaction, where the water produced in the process reacts with the CO and forms CO_2 and H_2, increasing the CO_2 emission of the system. On the other hand, Co-based catalysts have shown limited to no evidence of triggering the WGS reaction, and the selectivity of this catalyst is highly towards the hydrocarbon range that is used as the liquid fuel [12].

Co-based catalysts have been widely used for the FTS process [21], but for all catalysts, overheating of the system can cause them to lose activity due to the sintering of the metal on the support. Since the FTS is a surface reaction, when Co metal starts to sinter due to the high temperature in the system, it reduces the surface area for the reaction to take place; hence, a loss of catalyst productivity will occur [22]. In other words, poor temperature control can limit the productivity of the FTS catalyst. In the literature, it has been shown that the minimum lifespan of a Co-based catalyst needs to be on the order of years to be suitable for a commercial process [22]. This is because Co is expensive, and frequently replacing the catalysts is not desirable. The synthesis reaction itself is highly exothermic (ΔH = -164 kJ/mol) [23]; for this reason, proper heat management of the system and a proper understanding of how the heat transfer from the reaction during the synthesis process affects the system temperature are essential for the success of the FTS.

1.2.3 Computer model

Many studies suggest that the use of a diluent mix in the catalyst bed helps reduce the heat power density of the system, thus making temperature control easier [24]. However, the downside of mixing diluent with the catalyst is increased reactor size and cost. In order to reduce the heat density in the catalyst bed, a large amount of diluent, at least twice as much as the amount of

catalyst [25], is needed. Another way to reduce the cost and increase the time efficiency, besides doing numerous bench-top scale experiments in the lab, Computational Fluid Dynamics (CFD) tools can be used to predict the heat transfer performance of FTS reactors.

With the increase of computational power, CFD tools have become increasingly effective in simulating FTS for better predictions of this complex process. CFD tools help to predict the effect that different process variables (temperature, space velocity, CO/H_2 gas feed ratio, and pressure) have on the production of the FTS fuel.

As for the fixed bed reactor, several CFD modeling studies have been reported in literature. Wang et al. [26] developed a one-dimensional heterogeneous reactor model to simulate the performance of the reactor for hydrocarbon production, and a satisfactory agreement was reached between the model and the experimental system. Others have considered a two-dimensional pseudo-homogeneous model; Miroliaei et al. [11] simulated a fixed bed FT reactor using the discrete packing method to investigate the FTS process, and reported the effect of reaction temperature, feed flow rate, and H2/CO ratio on CO conversion and product selectivity. Irani et al. [27] developed and validated a 2-D CFD model with an optimized mesh to examine the hydrodynamic flow, chemical reaction, non-ideal mixture, and heat and mass transfer in the fixed bed reactor, and they reported 573 K as the optimum temperature of the system. Arzamendi et al. [23] used CFD to study the heat transfer in a microchannel reactor used for FTS.

Numerous CFD modeling studies have been reported in literature, and the effect of the process variables on the CO conversion and product selectivity have also been reported, but only a few studies have examined the control algorithms applied specifically to FTS. In 1988, Rohani et al. [28] implemented a self-tuning controller (STC) on a tube-wall reactor for FTS to control the

H_2/CO ratio of the inlet gas mixture and its flow rate. They investigated the set-point tracking and the rejection of the random deterministic disturbances. According to their results, the STC was able to reduce the variance of the process output by minimizing the error and disturbances in those feed gas rates. With the help of this higher level control algorithm, the product selectivity was more stable and precise, which increased the overall efficiency.

FTS is a well-known exothermic reaction, and the system temperature runaway is always a concern, especially in the beginning of the reaction when the catalyst activity is high. Loss of catalyst activity may result from overheating, so tight control of the temperature is desired. Over the years, several researchers have worked on different control strategies for controlling the exothermic reaction. Some researchers studied the different control methods to control a batch reactor. Arpornwichanop et al. [29] examined how model predictive control (MPC) and generic model control (GMC) can be used to control the temperature of a batch reactor. Karr et al. [30] researched how an adaptive generic algorithm fuzzy logic controller can control the reaction of formaldehyde reacting with ammonia in a continuously stirred tank reactor to produce hexamine and water. In addition, much research has studied how to implement an advanced control algorithm in a real pilot plant. Pinheiro et al. [31] and Afonso et al. [32] both used a linearized MPC to control a pilot plant reactor. In all of these studies, a physical system for testing and tuning was required.

However, from the survey of literature, none has been found that discusses the control algorithm for the system temperature control for FTS; in addition, no example was found that has examined how to use a simulation model coupled with a control algorithm to select and tune the controller used in the FTS process.

This dissertation aims to make use of available CFD tools to model heat transfer in an FTS reactor. The model will be then coupled with PID control algorithm to test the ability for the software to simulate the FTS system, and compare with the system used for experiment.

CHAPTER 2

FTS EXPERIMENT SETUP & OBSERVATIONS

For the experiment studied in this dissertation, a fixed-bed reactor was chosen because of the simplicity of the flow system, which can make the interpretation of the results easier. The catalyst used in the project was composed with Co on a silica support and Ru as a promoter.

This project was started as a means to improve an existing FTS experiment setup. The goal is to develop a method to simulate the FTS process with a controller system for further control study.

2.1 FTS Experimental Setup

In industry, natural gas is being reformed to produce syngas, which is a necessary element for the FTS process. Due to a limitation of time and resources, however, the creation of syngas by reforming is not considered. Instead, a carbon monoxide and hydrogen mixture was purchased from Airgas, a chemical gas company. A hood scale continuous flow fixed-bed FTS setup was designed and built as shown in Figure 1.

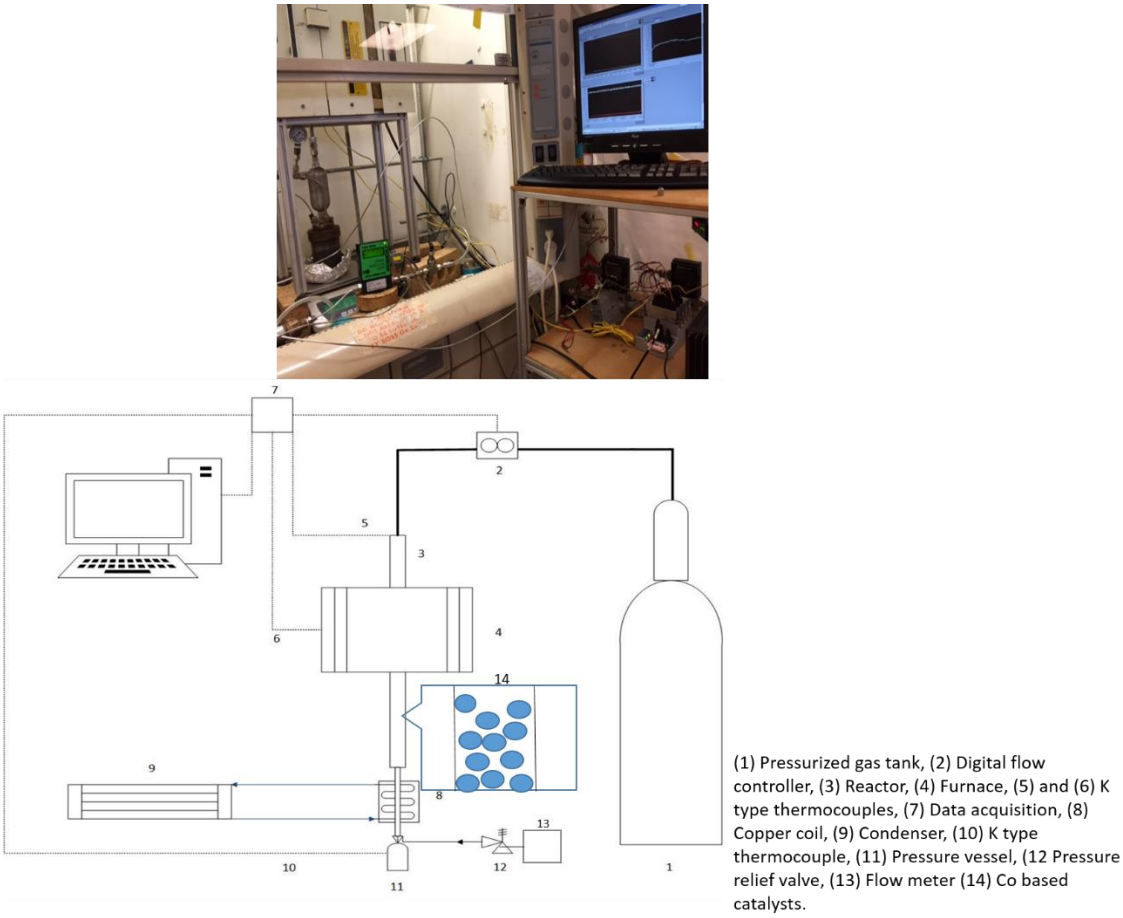

Figure 1. FTS Process Laboratory Scale Setup.

The prepared catalyst was placed in the mid-section of the carbon steel tube reactor with a length of 20 inches and inner diameter of 0.328 inches; the catalytic bed height was about 3 inches and was held in place with glass wool placed in both ends of the bed to prevent the bed from shifting during the process. A proportional-integral-derivative (PID) controlled electric furnace was used to maintain the desired reaction temperature. The reactor was placed in the furnace vertically with temperature controlled between 250 to 270 ˚C inside the reactor. Syngas (33% CO+ 67% H_2 on a mole basis) was being fed inside the reactor from the inlet at the top, the flow controller (Omega FMA 5400/5500 Mass Flow Control) was used to control the flow rate. The gas product from the outlet was condensed in a chamber at 4˚C to form liquid product that accumulated

at the bottom of a pressure vessel. A pressure relief valve was connected to the pressure vessel and set to maintain a pressure of 300 psig inside the system. The flow meter (Omega FMA 4000 Digital Mass Flow Meter) was used to monitor the outlet gas flow rate; the outlet gas sample was collected periodically for testing. A schematic diagram of the Fischer–Tropsch reactor unit is shown in Figure 1. A Labview data acquisition system (NI CDAQ-9174) was used to monitor the outlet flow rate and the temperature in various locations. Thermocouples were placed in three locations: (1) inside the reactor to determine the system temperature and used as the controller feedback signal, (2) in the pressure vessel to monitor the condenser temperature, and (3) on the inside surface of the furnace. All data was saved in the computer for further performance analysis.

2.2 FTS Experimental Results

The effect of different reactant flow rates on the reaction temperature was evident from the results. Figure 2 shows the temperature history for reactant flow rates of 100 SCCM and 300 SCCM. As seen from the temperature history plots, when the reactant flow rate fed to the system was 100 SCCM, the PID controller was able to maintain the set-point of the system. But as the reactant flow rate was increased to 300 SCCM, the PID controller was unable to hold the set-point temperature. It should be noted that the PID controller is a linear controller. There is no guarantee that a non-linear system can be controlled well by a linear controller. It is likely that at higher reactant flow rates, the FTS system is behaving more in a non-linear fashion. Therefore, a suitable controller with proper tuning is needed for a non-linear system.

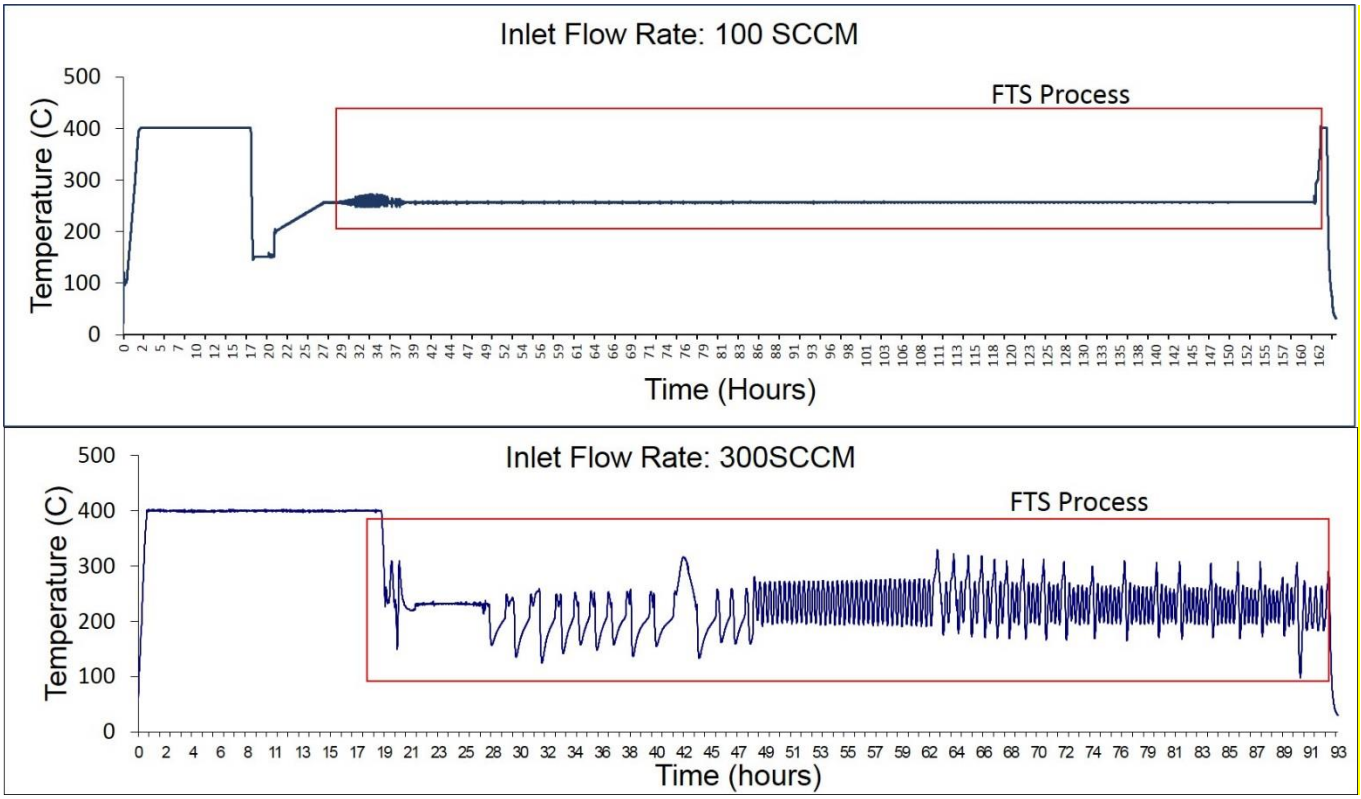

Figure 2. FTS Process Temperature History for 100 and 300 SCCM cases

At higher reactant flow rates, a significant overshoot of the set-point occurs. The effect of this overheating can been seen in catalyst characterization performed after the experiment. It is well known in the literature that high temperature can lead to sintering of the Co metal, thus reducing metal surface area [22].

The reduction of metal distribution can be seen from characterizing the catalysts with the use of a Transmission Electron Microscopy (TEM). Images were taken with TEM to capture the image of the Co metal distribution on the catalysts before and after the experiment. In the TEM technique, an electron emitted from the instrument passes through the thin specimen. As the electron passes through, it interacts with the specimen, and an image is formed on the basis of this interaction [33]. The TEM results are shown in Figure 3.

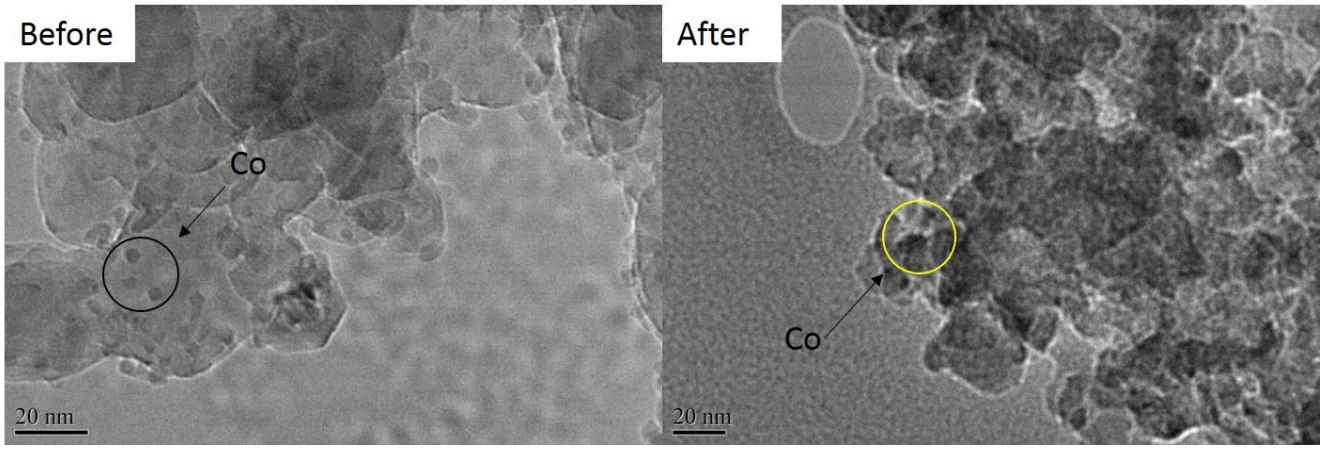

Figure 3. Catalyst Co Distribution TEM Image (image obtained by Pawarat Bootpakdeetam)

In Figure 3, the image on left was obtained from Co catalysts before the experiment with high system temperature, and the image on right was obtained after the experiment. By comparing both images, the catalyst before the experiment image shows a more spread out distribution of the Co metal, as the Co appears to be thinner across the surface. For the catalysts after the experiment, the sintering resulted in larger Co clusters and a darkening of the image across the area of interest.

From the results above, it was shown that high temperatures have an effect on the Co-based catalyst. A properly tuned controller that can maintain system temperature at high flow rate is desired.

2.3 Motivation

In the FTS, the maximization of catalyst productivity is a major objective. The production rate is determined by the activity of the catalyst, which is temperature dependent, and the syngas flow rate into the system. Since reaction temperature is a fixed variable, productivity can be improved by increasing reactant flow rate. However, experiment results given in section 2.2 show difficulty in holding the system temperature at a high flow rate. It is possible that the system is becoming more non-linear as the flow rate increases, and has become incompatible with a PID

controller, or maybe it is simply because the parameters used for the PID algorithm needed to be tune to optimize the controller's performance.

Controller tuning is usually done by trial and error on the physical system. However, FTS reaction is a very slow process. Running the physical system requires a significant amount of time to prepare the catalysts, setup, and run the experiment, before results may be collected. In addition, it may be dangerous if the controller fails and the system becomes unstable. However, due to the advancement in computing power, the FTS process can be simulated and the model can be used to select a suitable control system, so a physical experiment is not needed for turning the controller.

With the goal to develop a simulated system for the FTS system temperature, a study of a simulation platform was developed. A multi-platform coupled simulation using ANSYS-FLUENT and MATLAB/Simulink was established to simulate the FTS process coupled with PID control algorithm to reflect the system temperature behavior of the FTS system as preformed in the experiment.

2.4 Objectives

The first objective of this dissertation is to establish a multi-platform coupled simulation to simulate a flows in a reactor coupled with a PID control algorithm. The second objective is to develop a detailed FTS kinetic model with the experiment data obtained in the FTS process. The third objective is to couple the FT kinetic model to the multi-platform developed earlier, and run a simulation for the FTS system combined with the PID controller. The purpose of establishing this multi-platform coupled simulation is to predict the system behavior though simulation in order to further study the control algorithm uses to control the system temperature.

2.5 Contribution

Over the years, several researchers have worked on different strategies for controlling exothermic reactions [28, 29, 30, 31]. In addition, many studies have successfully developed simulation models for the FTS process, and significant agreement between these computational models and experimental results have been reported [22, 26, 11, 25]. However, no literature found has investigated the performance of a control algorithm specifically used to control the FTS system temperature.

Therefore, the guidelines taken from these studies support the efforts of this dissertation to develop a simulation model and couple it with a control algorithm that uses data files sharing. The developed simulation platform can be used to investigate how to control a system with a highly exothermic reaction.

The results of this study show that the performance of a control algorithm can be rapidly tested with the developed simulation platform. The results also show that CFD tools can be used to simulate the heat transfer characteristic of systems for control study. Finally, the results show that the platform provides the ability to properly tune the controller before implementing it in the physical system, which can reduce costs, increase time efficiency, and eliminate the need to do numerous bench-top scale experiments in the laboratory.

2.5.1 Publications

"Simulation Platform for Rapid Testing of Methods to Control Exothermic Chemicals Reactions", ASME 2015 IMECE, Houston, TX.

CHAPTER 3

SOFTWARE SYSTEM

In this dissertation, a coupled simulation platform with ANSYS-FLUENT and MATLAB was developed. The model is simulated in ANSYS-FLUENT and the control algorithm is executed in MATLAB.

The two software packages exchanged data via a shared file system, thus allowing each package to run on a separate computing platform. This multi-platform coupled simulation framework enabled the investigation of different control techniques used to maintain the temperature of the system as a function of the process reaction rate. The results verify the feasibility of using such a platform to test different control algorithms for a temperature control problem.

3.1 Coupled Platform Structure

The communication between ANSYS-FLUENT and MATLAB is the most important factor for this platform to be able to operate successfully. In this dissertation, a method for the data transmission between these two software packages is presented. In MATLAB, SIMULINK can be used to perform complex control system simulations, and by S-function written in C programming language, SIMULINK can be set to perform user customized tasks. In ANSYS-FLUENT, a journal file can be created with all the necessary commands required by ANSYS-FLUENT, including a command to instruct ANSYS-FLUENT to output the simulation result to a file that can be accessed by both MATLAB and ANSYS-FLUENT. To deal with the unsteady boundary condition in ANSYS-FLUENT, a user defined function (UDF) written in C programming language can be used to set the boundary condition parameter upon the specific time step. With the use of C

programming and the extended functions in MATLAB and ANSYS-FLUENT, data exchange was realized in this dissertation.

ANSYS-FLUENT simulates the reacting flow and computes the temperature in the flow field according to the initial conditions, boundary conditions, and the source term set through a UDF. Next, MATLAB reads the data from ANSYS-FLUENT and computes the corresponding output signal in SIMULINK. When the output signal is received, ANSYS-FLUENT refreshes the boundary condition and computes the result for the next time step. This process repeats at each time step until the final time step is reached. The implementation of the entire simulation process is shown in Figure 4.

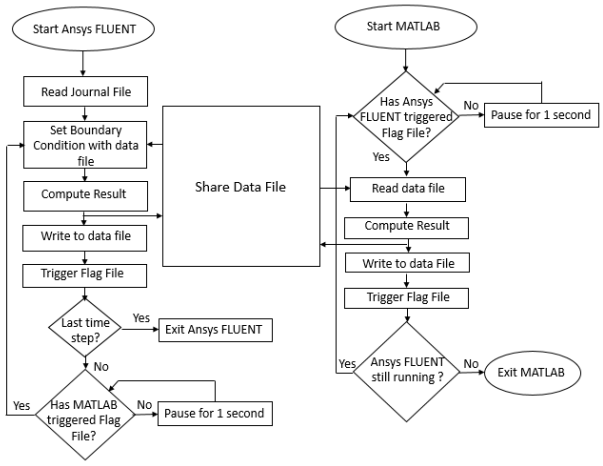

Figure 4. Simulation Flow Chart

ANSYS-FLUENT and MATLAB communicate by reading the shared data file and triggering the flag file alternatively from the start, and they exchange data in the process as shown in Figure 4. The main steps are described as follows:

1. ANSYS-FLUENT and MATLAB run simultaneously in the beginning. ANSYS-FLUENT reads the Journal file, prepares the model, sets parameters, and computes the result. During this process MATLAB waits for the flag file to be triggered by ANSYS-FLUENT.
2. After ANSYS-FLUENT computes the result, it triggers the flag file and MATLAB inputs the data from the shared data file into the control system and computes the required control signal. Then MATLAB triggers the flag file to inform ANSYS-FLUENT.
3. ANSYS-FLUENT is informed by the second trigger and reads the data from the shared data file and refreshes the boundary condition with the new data from MATLAB and computes the new result.

This cycle between the two software packages continues for the number of time steps provided by the user.

CHAPTER 4

SOFTWARE SYSTEM TESTING

In this chapter. a simple test case was created to demonstrate the function of this multi-platform system. A simple tubular reactor was modelled in ANSYS-FLUENT and was coupled with the Proportional-Integral-Derivative Control (PID) control algorithm in MATLAB.

4.1 Problem Definition

To maintain the desired temperature within the system, the model's boundary temperature, which is also defined as the temperature input of the system, was controlled with a feedback signal obtained by the temperature sensor located inside the reactor. Figure 5 shows the reactor geometry and the location of the temperature sensor. In the ANSYS-FLUENT simulation model, the boundary temperature was applied to the domain's wall, and the temperature at the center of the reactor was measured. This measurement was then passed on to the controller in MATLAB to calculate the error value, and produce the next required control temperature to be used as a boundary temperature for the next time step for the model. In this case, error was defined as,

$$e(t) = T_{SP} - T_{meas}(t) \tag{4.1}$$

Where e(t) is the error of the system measurement, T_{SP} is the set-point temperature, and $T_{meas}(t)$ is the measured temperature.

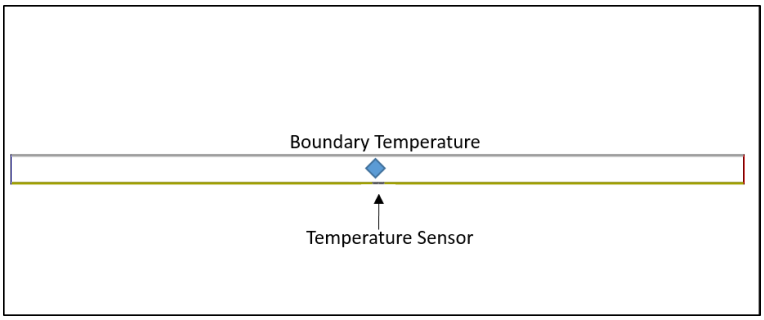

Figure 5. Reactor Model with Temperature Sensor Location

4.2 ANSYS-FLUENT Model

In this dissertation, a single tubular reactor was used to contain the reacting flow as it has the capability to effectively remove heat and has a uniform heat transfer rate along the radial direction.

4.2.1 Geometry and Mesh

Because of the symmetry of the reactor tube, a domain of only half of the cross section surface along the reactor was needed, which reduces the required computing time. A mesh for the entire reactor domain was obtained by revolving the calculated zone along the defined center line of the reactor. The 2-D axisymmetric model with a radius of 0.0127 m and a length of 0.508 m was created with a uniform coarse mesh applied to it.

A grid was generated with cell clustered toward the wall to capture the thermal boundary layer as shown in Figure 6. The mesh contained 3000 cells and 3216 nodes.

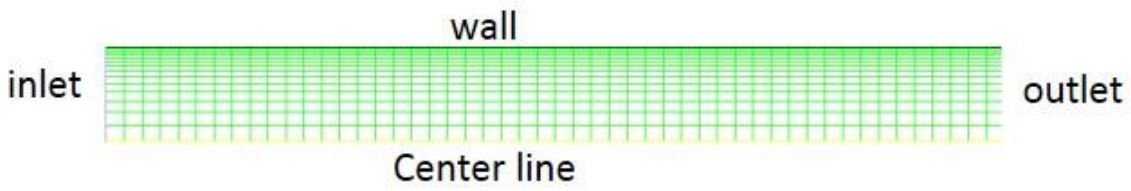

Figure 6. Refined Reactor Grid

4.2.2 Conservation Equations

The governing equations being solved in ANSYS-FLUENT were the mass conservation equation, momentum conservation, species transport equation, and energy equation for an incompressible transient reaction flow [34]. They can be expressed as:

Mass conservation:

$$\nabla \cdot \vec{v} = 0 \tag{4.2}$$

Momentum conservation:

$$\rho(\frac{\partial \vec{v}}{\partial t} + \vec{v} \cdot \nabla \vec{v}) = -\nabla \cdot P + \mu \nabla^2 \vec{v} \tag{4.3}$$

Species transport equation:

$$\nabla \cdot (\rho_i \vec{v} Y_i) = -\nabla \cdot \vec{J}_i + R_i \tag{4.4}$$

Energy equation:

$$\rho C_p \left(\frac{\partial T}{\partial t} + \vec{v} \cdot \nabla T\right) = S_R(T) + \mathrm{k}\nabla^2 T \tag{4.5}$$

Where t is the time, ρ is the density, C_p is the heat capacity, $\vec{v}$ is the velocity vector, P is the static pressure, μ is dynamic viscosity, k is the thermal conductivity, T is the temperature, R_i is the

reaction rate of species i, Y_i and J_i are the mass fraction and diffusion flux of species i. As a simplification, all material properties are assumed to be constant.

The function S_R is a temperature dependent reaction term and is defined as

$$S_R = AT^n, A = \begin{cases} 1.0 & for\ T \geq T_{act} \\ 0.0 & for\ T < T_{act} \end{cases}, \tag{4.6}$$

where *n* is an arbitrary parameter that is used to control the degree of non-linearity at the reaction term. T_{act} is the reaction activation temperature, and from the studies, the FTS reaction activation temperature was found to be around 493K. Therefore, for cases presented, T_{act} was set to be 493K. This simple model allows one to control the degree of reactivity of the model.

Usually the magnitude of the heat source is calculated based on the different types of chemical reaction. But for this simplified test case, the heat source S_R applied to the model was reduced to a simple exponential function. This simplified heat source was used to serve as the purpose of mimicking some of the major characteristics of the FTS reaction, which were: (1) the reaction only occurred when T_{act} was reached and (2) the thermal energy came from the reaction was a non-linear function.

The SIMPLE [35] scheme was used to couple the velocity and the pressure, and second order upwind method was selected for the momentum and energy equation.

4.2.3 Parameter n Selection

In this section, the method for selecting a range of test cases with different n is presented. To be controlled successfully, thermal systems depend on the system's capability to remove or add the precise amount of heat to or from the system. In this model, the wall temperature (T_{wall}) is adjusted by the controller. This allows for cooling or heating of the model depending on the value

of T_{wall}. When the reaction starts, the controller will output the most optimum wall temperature for the system to maintain at the set-point temperature. However, despite the controller output temperature, the maximum heat the system can practically remove is limited by the thermal characteristics of the system.

In order to provide a rough calculation of the amount of heat that the system can remove, a simplified, 0-D model was used, which can be described by the equation,

$$\dot{T} = \frac{1}{\rho C_p V}\left[\dot{m}C_p(T_{in} - T_{out}) + AT^n V - k\frac{T_{wall}-T_{meas}}{l}A\_surf\right] \quad (4.7)$$

where, A is a constant, $\dot{T}$ is the rate of change of temperature, ρ is the density of the fluid, C_p is the heat capacity, V is the reactor volume, $\dot{m}$ is the mass flow rate, T_{out} is the temperature at the outlet, T_{in} is the temperature of the input gas, k is the coefficient of thermal conductivity, *A_surf* is the surface area, l is the reactor wall thickness, and T_{meas} is the temperature measured by the thermocouple inside the reactor, and which is assumed to be equal to T_{out} in this lump mass model.

The heat convection in the model can be ignored if the following condition was satisfied [36],

$$Pe\frac{H}{L} \ll 1 \quad (4.8)$$

Where H is the height of the reactor, L is the length of the reactor. Pe is the Péclet number of the system. The Péclet number is a dimensionless number used for the measurement of the ratio between the heat convection and the heat conduction in a system [36]. If equation (4.8) was satisfied, the majority of the heat in the system is transferred by conduction, and the heat transfer causes by convection can be ignored.

The value for equation (4.8) was calculated to be 0.045 in this system, therefore, the heat power passed through the reactor wall via only conduction as,

$$q_{reactor} = -k\frac{T_{wall}-T_{meas}}{l}A\_surf\ - \dot{m}C_p(T_{in} - T_{meas}) \tag{4.9}$$

where $q_{reactor}$ is the integrated heat flux on the reactor's wall, h_c is the coefficient for convection. For the reaction term, the power is,

$$q_{reaction} = -AT_{meas}^{n}V \tag{4.10}$$

where T_{meas}^{n} is the reaction term in W/m^3.

To estimate amount of heat the system can remove, $q_{reactor}$ needs to be equal to $q_{reaction}$. Therefore, equation (4.9) and (4.10) become,

$$AT_{meas}^{n}V = k\frac{T_{wall}-T_{meas}}{l}A\_surf\ + \dot{m}C_p(T_{in} - T_{meas}) \tag{4.11}$$

as T_{meas} is maintain at the set-point temperature. Finally, equation (4.11) is defined as,

$$n\ log(T_{meas}) = \log\left[\frac{k\frac{T_{wall}-T_{meas}}{l}A\_surf\ + \dot{m}C_p(T_{in}-T_{meas})}{AV}\right] \tag{4.12}$$

and to solve for n,

$$n = \frac{\log\left[\frac{k\frac{T_{wall}-T_{meas}}{l}A\_surf\ + \dot{m}C_p(T_{in}-T_{meas})}{AV}\right]}{log(T_{meas})} \tag{4.13}$$

The values for all the parameters used in equation (4.13) are shown in Table 1 below.

Table 1. Parameters' Values for 'n' equation

Parameter	Value
k	$3.2\text{x}10^{-2}$ [W/m-K] (air)
l	$1.27\text{x}10^{-2}$ [m]
A_surf	$4.05\text{x}10^{-2}$ [m^2]
V	$2.57\text{x}10^{-4}$ [m^3]
T_{meas}	528[K]
T_{wall}	298 [K]
$\dot{m}$	$1.8\text{x}10^{-6}$ [kg/s]
C_p	1020[J/kg-K]
T_{in}	298 [K]
A	1.0 $for\ T \geq T_{act}$ 0.0 $for\ T < T_{act}$

Using equation (4.13), the n value calculated is 1.8. However, this is only a rough estimation for the *n* parameter using a lump mass model of the system. Therefore, a range of cases were also considered to better test the reaction characteristic of the system. The selected *n* values for testing were $n = 1.4, 1.5, 1.6, 1.7,$ and *1.8.*

4.2.4 Boundary Conditions

Figure 6 shows the defined boundary conditions. The inlet flow rate of the system was set to 100 SCCM (Standard Cubic Centimeters per minute) of air at room temperature. The flow inside the reactor was laminar with a Reynolds number of 111. The Mach number is 9.6×10^{-6}, so the flow was assumed incompressible. A no-slip condition was applied to the wall due to the presence of viscosity of the fluid, and the center line was set to symmetry. A transient flow calculation was used because of the time varying temperature boundary condition.

A uniform temperature was specified on the wall with a User defined function (UDF). The wall temperature is a function of time and is determined at each time step by the control algorithm running in MATLAB.

4.2.5 User Defined Function

In ANSYS-FLUENT, user customized tasks can be executed by creating User Defined Functions (UDFs) which are then compiled in the simulation. Two UDFs were created for this platform. One UDF was for the reaction term in the energy equation and the other for the wall boundary temperature.

The reaction term, S_R, in Equation 4.6 was linearized about the temperature obtained from the previous time step and then implemented in the UDF as a source term for the energy equation. The second UDF was used to apply the wall boundary condition to the model.

At each time step, ANSYS-FLUENT collected the output temperature calculated from the MATLAB controller program and then applied to the wall as the boundary condition for that time step. As of the simulation finished, the output temperature resulted from the simulation was collected, and sent to the MATLAB for the calculation of the temperature for next time step.

ANSYS-FLUENT and MATLAB continued to exchange data in this fashion to keep the simulation and the controller synchronized.

4.3 PID Control Model

Controller models were developed in MATLAB/Simulink and were coupled with the ANSYS-FLUENT simulation. A PID control model was developed to investigate the controllability for the ANSYS-FLUENT model as a function of the model non-linearity parameter, n.

A program containing a PID algorithm was written and executed as a controller for the system being simulated in ANSYS-FLUENT. The PID controller was chosen to be the baseline of this system, since this controller is widely used in situations where a system needs to be controlled based on the feedback signal.

A PID controller minimizes the error between the desired set-point value and the actual system output value (the feedback signal). This is done by calculating the output signal as follows,

$$u(t) = k_p e(t) + k_i \int e(t)\,\mathrm{d}t + k_d \frac{\mathrm{d}e}{\mathrm{d}t} \tag{4.14}$$

where $u(t)$ is the output temperature, $e(t)$ is the error signal measured between the desired set-point and the measured temperature, k_p is the proportional gain, k_i is the integral gain, and k_d is the derivative gain. These three gains combined with the tracking error signal determine the proper output temperature for the system in the next time step.

In order to solve this time continuous function in a discretized time system, the function u(t) needs to be discretized.

For the differential function from u(t),

$$D(t) = k_d \frac{\mathrm{d}e}{\mathrm{d}t} \tag{4.15}$$

where $D(t)$ is the output of the differential function. The first order method was used to discretize $D(t)$ into the following function,

$$D(t) = k_d\left(\frac{e_i^n - e_i^{n-1}}{\Delta t}\right) \tag{4.16}$$

where Δt is the size of time step, and $e_i^n - e_i^{n-1}$ is the difference in tracking error between the current time step and the previous time step. To discretize the integral function, the Trapezoidal Rule was used to approximate the integral of $\int e(t)\,\mathrm{d}t$,

$$\int e(t)\,\mathrm{d}t = \frac{(e_i^n + e_i^{n-1})\Delta t}{2} \tag{4.17}$$

When these transformations are complete, the continuous time u(t) function becomes a discretized time function and can be evaluated at each time step.

4.4 Results

For all cases, the duration for each simulation run was 50 seconds. For each case, the measured temperatures, T_{meas}, were plotted against time in seconds.

In this dissertation, different values of n were tested and the goal was to determine the limitation on the PID controller. In general, PID controllers are limited to the control of linear systems. However, for low values of n, the non-linearity of the reaction term is not strong, so the PID controller may operate acceptably. This study identifies the values of n that lead to unacceptable PID results.

PID controllers perform best when they are tuned. PID tuning is the process to minimize the error of determining the values of the gains (k_p, k_i, k_d) in the controller. Many methods as to how to systematically obtain the gains have been studied; however, for this dissertation, the Ziegler–Nichols close loop tuning method [37] was used with this method, if the system is not able to settle on a value within 5% of the desired set-point temperature, the case is considered "not PID controllable."

The Ziegler–Nichols closed loop tuning method was developed by John G. Ziegler and Nathaniel B. Nichols [38]. The tuning process begins by first setting the integral gain and derivative gain on the controller to zero. Next, the proportional gain is increased until it reaches the ultimate gain, defined as when the output of the system signal displays an oscillatory behavior with a constant amplitude. Finally, with the values of ultimate gain and the oscillation period, the integral gain and derivative gain can be set accordingly [38].

In this dissertation, the tuned controller was applied to the reaction model for different values of n. The results are shown in Figure 7 and Figure 8. The results show that the PID controller was able to maintain the measured temperature within 5% of the set-point temperature when n is less than 1.7.

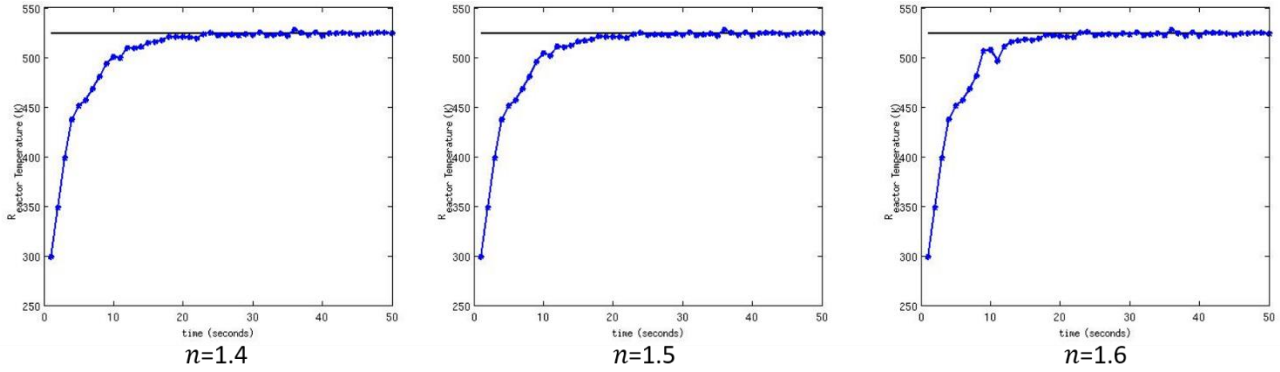

Figure 7. Low n Value PID Results

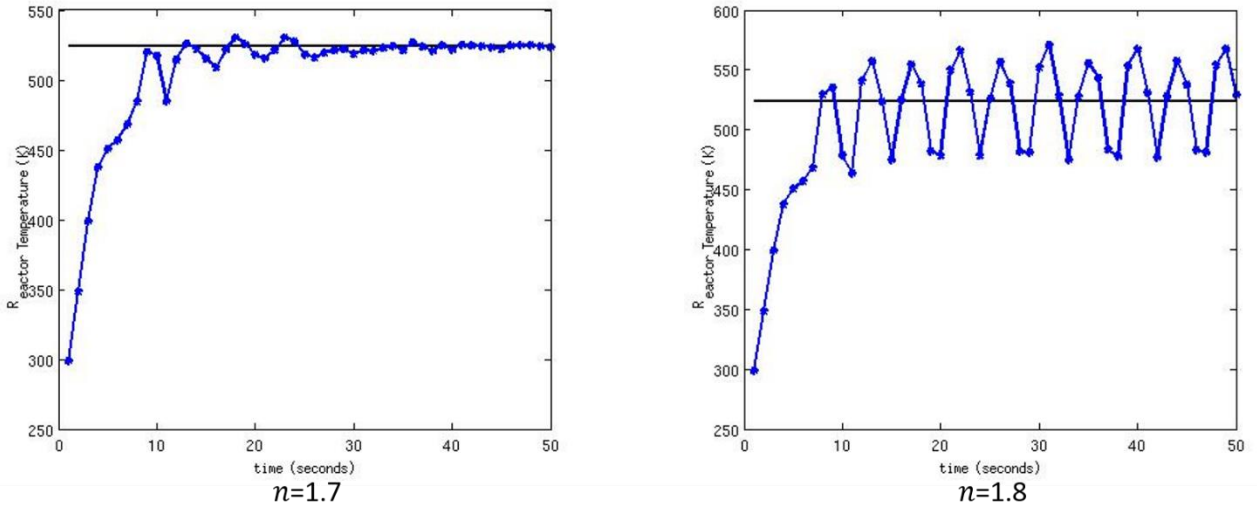

Figure 8. High n Value PID Results

The case of n = 1.7 shows a small amount of overshoot in the response at the beginning, but this was damped and the temperature reached a steady state in about 40 seconds. Despite the fluctuation of temperature in the beginning, the overall temperature never went above 5% of the desired set-point. Therefore, the results shown in the above cases demonstrate that the PID controller was able to achieve the desired set point when the non-linearity of the reaction term was not strong.

As n was increased beyond 1.7, the PID controller did not perform well. Figure 8 also shows the PID response for the case of n = 1.8. The response had a constant oscillation about the set-point, the PID controller was unable to eliminate this oscillation from the system. Therefore, the PID method results in higher error as the non-linearity of the reaction term of the model increases.

4.5 Summary

In this section, a simple test case was defined to demonstrate the implementation of the multi-platform system. For this test case, the reactor was modeled as a 2-D axisymmetric domain because of the symmetry shown in the reactor tube. Because a grid with clustered cells near the wall was generated in the domain, the thermal boundary layer was better captured in the simulation. The domain was imported into ANSYS-FLUENT. In addition, the governing equations for the domain were solved in ANSYS-FLUENT. A temperature dependent reaction term was added to the energy equation to control the level of reactivity of the model by the parameter *n*. Two UDFs were created in ANSYS-FLUENT: one UDF was used to introduce the reaction term into the energy equation, and the other UDF was used to uniformly apply the controlled temperature on the wall of the domain. For the system temperature control, a discretized PID control algorithm was written in .m file format and compiled in MATLAB.

Models with different levels of reactivity were tested with the PID controller; the results show that the PID controller was able to handle models with low reactivity, but as the reactivity in the model increased, the controller failed to handle it. For the model with the highest reactivity, the results show a constant temperature oscillation about the set-point temperature, and the PID controller was not able to eliminate this oscillation from the system nor maintain the temperature at the set-point temperature. However, for this test case, the results show that the developed multi-

platform system could be used to couple the model simulated in ANSYS-FLUENT and the PID controller compiled in MATLAB.

CHAPTER 5

FTS MODEL VALIDATION

The simulation studied in this dissertation was set up using ANSYS-FLUENT. An FTS system modeled and solved by finite volume method from the literature [3] was reproduced in this dissertation using the commercial CFD software ANSYS-FLUENT to validate the FTS model and this simulation. In addition, the results from both simulations were compared.

5.1 Porous Media Model

For the simulation of the reactor model with a packed catalyst bed, instead of individually modeling the catalyst pellets inside the reactor, a continuum of the catalyst with a reduced density, or a porous media, was modeled inside the reactor domain [39].

5.1.1 Porosity

A porous media consists of a network of pores contained in a material or some control volume. Therefore, for calculation, the volume fraction between the void and the solid in a material is more meaningful than the mass fraction of the material [40]. The volume fraction presented in a material or a control volume is referred to as the porosity. Porosity is a dimensionless variable with values that range from 0 to 1, where the value of 1 represents that the control volume is 100% unobstructed. Porosity can be calculated [41] as,

$$\varepsilon = \frac{V_{pore}}{V_{CV}} \tag{5.1}$$

Where ε is the porosity, V_{pore} is the volume of the pores existing in a material, and V_{CV} is the volume of the control volume.

Two types of voids exist inside the reactor for FTS. With a packed catalyst bed inside the reactor, they directly affect the porosity of the system. These are defined as the void between the catalyst pellets and the void inside an individual catalyst pellet.

The void between the catalyst pellets is mainly affected by the shape of the catalyst itself and the method of packing the catalyst into the reactor. A catalyst bed with pellets of high sphericity and low roundness has a low porosity [41]. The sphericity is a 3-D measure of how spherical an object is, meaning the higher the sphericity of the pellet, the more sphere-like the pellet is. Roundness is a 2-D measure of how smooth an object's edge is, meaning the higher the roundness of an object, the more circle-like that object is. Figure 9 shows objects with different levels of roundness and sphericity. The figure also illustrates the relationship between the shape of the object and the porosity of the system with the packed object.

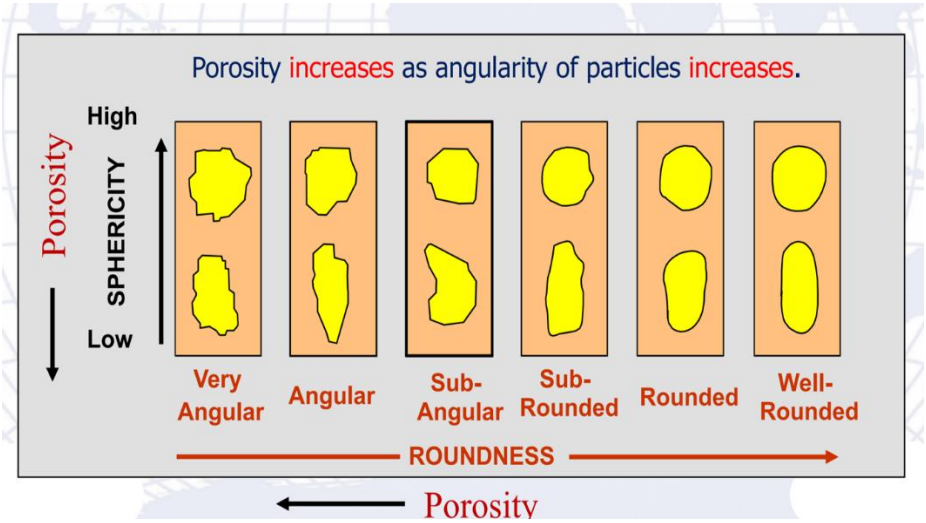

Figure 9. Particles Porosity (image taken from Ned. University of Engineering & Technology)

The other factor of the porosity for the catalyst bed is the void that exists inside an individual catalyst pellet. Catalyst pellets have many pores or channels inside their structures to maximize the surface area for the reaction to occur while maintaining the strength of the structure.

The pore diameter inside the catalyst pellet is usually represented in Armstrong units and cannot be seen by the human eye, so the catalyst porosity needs to be determined by a Brunauer–Emmett–Teller (BET) Analyzer. The BET Analyzer measures the specific surface area and pore volume of a catalyst pellet by determining the physical adsorption of gas on the surface of the catalyst and the amount of the adsorbate gas corresponding to a monomolecular layer on the surface [27]. Using the two different types of voids previously discussed, the final porosity within a catalyst bed can be defined as,

$$\varepsilon = \frac{(V_{reactor} - uV_{cat.}) + uV_{BET}}{V_{reactor}} \tag{5.2}$$

Where $V_{reactor}$ is the volume of the reactor, $V_{cat.}$ is the volume of a catalyst pellet, V_{BET} is the pore volume inside a pellet determined by BET analysis, and u is the number of catalyst pellets packed inside the reactor.

For simulation, the catalyst bed is modeled as a continuum of the catalyst, therefore, no catalyst pellets are modeled inside the reactor that can provide the inertial and viscous resistance to the flow. The porosity of the catalyst bed is used as a decreasing factor for the fluid velocity, so the model can achieve the same mass flow rate in the bed as if the catalyst pellets was modeled inside the reactor [39]. This decreased velocity is also called the superficial velocity, which is defined as the fluid velocity corrected by the porosity,

$$\vec{v}_s = \frac{\vec{v}}{\varepsilon} \tag{5.3}$$

Where v is the velocity of the fluid, $\vec{v}_s$ is the superficial velocity, and ε is the porosity. From this equation, when the porosity is equal to 1, meaning 100% voidage within the material, $\vec{v}$ is equal

to $\vec{v}_s$. This mean the velocity of the fluid, $\vec{v}$, needs to be determined when the control volume is unobstructed.

5.1.2 Governing Equations

For the porous media, the governing equations are written as [42],

A. The continuity equation, or the conservation of mass,

$$\frac{\partial \rho}{\partial t} + \nabla \cdot (\rho\, \vec{v}) = 0 \tag{5.4}$$

B. The momentum conservation equation,

$$\frac{\partial}{\partial t}(\rho \vec{v}) + \rho(\frac{\partial \vec{v}}{\partial t} + \vec{v} \cdot \nabla \vec{v}) = -\nabla \cdot P + S_i \tag{5.5}$$

Where S_i is the source term for modeling porous media.

A porous media domain is modeled by adding the momentum source term, S_i, to the standard momentum conservation equation to reflect the pressure drop caused by the porous media. This source term is composed of two parts: the viscous loss term and the inertial loss term. The general form of this source term is written as,

$$S_i = \frac{\mathrm{d}P}{\mathrm{d}L} = -(\sum_{j=1}^{3} D_{ij} \mu \vec{v}_j + \sum_{j=1}^{3} C_{ij} \frac{1}{2} \rho |\vec{v}| \vec{v}_j) \tag{5.6}$$

Where $|\vec{v}|$ is the magnitude of the velocity vector, S_i is the source term for the i^{th} momentum equation, L is the length of the domain, and D_{ij} and C_{ij} are prescribed matrices.

As for a simple homogeneous porous media, the source term can be reduced to,

$$S_i = \frac{\mathrm{d}P}{\mathrm{d}L} = -(\frac{\mu}{\alpha} \vec{v}_i + B_2 \frac{1}{2} \rho |\vec{v}| \vec{v}_i) \tag{5.7}$$

Where α is the coefficient of permeability, and B_2 is the inertial resistance factor.

Moreover, the pressure drop of the porous media can be calculated by knowing the coefficient of permeability for the object. Permeability is defined as the ability of a porous media to transmit fluids, and it is calculated using the porosity of the object and the superficial velocity of the fluid. The coefficient of permeability can be related to pressure drop in the reactor by using Darcy's law [40],

$$\vec{\mathrm{q}} = \frac{-\alpha}{\mu}\nabla P \tag{5.8}$$

Where α is the coefficient of permeability, $\vec{\mathrm{q}}$ is the Darcy flux, and ∇P is the pressure gradient vector, which is also the pressure drop per length in this case. Therefore, the above equation can be rewritten as,

$$\frac{\mathrm{d}p}{\mathrm{d}L} = \frac{\mu}{-\alpha}\vec{\mathrm{q}} \tag{5.9}$$

Furthermore, in ANSYS-FLUENT, for a simple homogeneous porous media domain, the momentum source term representation is given in [43] and is defined as,

$$S_i = \frac{\mathrm{d}P}{\mathrm{d}L} = R_v \mu \vec{v}_s + \frac{R_n}{2}\rho \vec{v}_s |\vec{v}_s| \tag{5.10}$$

Where R_v is the viscous resistance and R_n is the inertial resistance, μ is the viscosity of the main fluid, and L is the length of the porous media bed. In addition, the pressure drop per length for the porous media within a fluidized bed can be calculated using the Ergun equation [44],

$$\frac{\Delta \mathrm{P}}{L} = \frac{150\mu(1-\varepsilon)^2}{\phi^2 D_p^2 \varepsilon^3}\vec{v}_s + \frac{1.75\rho(1-\varepsilon)}{\phi D_p \varepsilon^3}\vec{v}_s|\vec{v}_s| \tag{5.11}$$

Where D_p is the diameter of the pellet, ρ is the density of the fluid, and ϕ is the sphericity of the pellet. By comparing the Ergun equation to the momentum term defined in ANSYS-FLUENT, the inertial resistance and the viscous resistance can be defined.

As previously discussed, sphericity is the measure of how spherical an object is, and sphericity can be calculated by [45],

$$\phi = \frac{6V_p}{D_p S_p} \tag{5.12}$$

Where V_p is the volume of the pellet, S_p is the surface area of the object, and D_p is the equivalent diameter of the object. Equivalent diameter is the diameter of a sphere that has the same volume as the object being measured; therefore, D_p can be written as,

$$D_p = 2r_s \tag{5.13}$$

Where r_s is the radius of the equivalent sphere and can be determined by,

$$r_s^3 = \frac{3V_p}{4\pi} \tag{5.14}$$

C. The Species Transport Equation

The conservation equation for the chemical species inside the porous media is written as,

$$\frac{\partial}{\partial t}(\rho Y_i) + \nabla \cdot (\rho \vec{v} Y_i) = -\nabla \cdot \vec{J}_i + R_i \tag{5.15}$$

Where Y_i is the local mass fraction of each species, R_i is the net rate of production of species *i* by chemical reaction, and J_i is the diffusion flux of species *i*. The diffusion flux of species *i* can be determined by [46],

$$\vec{J}_i = \frac{\rho M_i}{M^2} \sum_{j=i} M_j D_{ij} \nabla x_j \tag{5.16}$$

Where D_{ij} is the diffusivity coefficient, M_i is the molecular weight of the species *i*, M is the molecular weight of the mixture, and x is the mole fraction.

To simulate chemical reactions inside a domain, the reactions are assumed to be volumetric and occurring throughout the domain [43, 39]. This assumption is valid only when the catalyst pellet size is small and the main focus concerns the changes in the concentrations of a species in length scale [39]. The species react with others through molecular diffusion within the domain. In this Chapter, the diffusivity coefficient between each species was determined using the kinetic theory. In addition, to apply the kinetic theory to the model, ANSYS-FLUENT uses the modified Chapman-Enskog [43] to compute the diffusivity coefficient,

$$D_{ij} = 0.00188 \frac{[T^3 (\frac{1}{M_{w,i}} + \frac{1}{M_{w,j}})]^{1/2}}{P_{abs} \sigma_{ij}^2 \Omega_D} \tag{5.17}$$

Where M_w is the molecular weight, P_{abs} is the absolute pressure in the system, Ω_D is the diffusion collision integral, and σ_{ij} is the arithmetic average of the individual molecular radius defined by,

$$\sigma_{ij} = \frac{1}{2}(\sigma_i + \sigma_j) \tag{5.18}$$

Ω_D is a function of the dimensionless temperature T^*,

$$T^* = \frac{k_B T}{\epsilon_{12}} \tag{5.19}$$

Where k_B is the Boltzmann constant, and ϵ is a molecule specific parameter. The values of the molecule specific parameter can be found in the [47, 48] and the ANSYS-FLUENT material database. The correlation between Ω_D and T^* can be found as [48],

$$\Omega_D = \frac{1.16145}{T^{*0.14874}} + \frac{0.52487}{\exp(0.77320T^*)} + \frac{2.16178}{\exp(2.43787T^*)} \quad (5.20)$$

D. Energy Equation

For a porous media domain, the standard energy equation is modified to include the conduction flux and the transient term. An effective conductivity is used for the conduction flux, and in the transient term, the thermal inertia of the solid phase is also considered. The energy equation for porous media can be written as,

$$\frac{\partial}{\partial t}\left(\varepsilon\rho_f E_f + (1-\varepsilon)\rho_s E_s\right) + \nabla\cdot\left(\vec{v}\left(\rho_f E_f + \mathrm{P}\right)\right) = \nabla\cdot\left[k_{eff}\nabla\mathrm{T} - \left(\sum_i h_i\vec{J_i}\right)\right] + S_f^h \quad (5.21)$$

Where E_f is the total fluid energy, E_s is the total solid medium energy, S_f^h is the fluid enthalpy source term, h_i is the enthalpy of the species, and k_{eff} is the effective thermal conductivity. In addition, the effective thermal conductivity in porous media is defined as,

$$k_{eff} = \varepsilon k_f + (1-\varepsilon)k_s \quad (5.22)$$

Where k_{eff} is the effective conductivity, k_f is the conductivity of the fluid, and k_s is the conductivity of the solid media.

5.2 Properties of Mixture Fluid

As the reaction inside the domain begins, the reactant species are consumed, and the amount of the product species increases. Therefore, the components of the mixture fluid are changing as a function of time and their location along the reactor. In this dissertation, due to the low Reynolds number (Re << 2300) inside the reactor, the flow was considered to be laminar [40]. Therefore, the densities of the individual species were considered to be constant throughout the

domain due to the incompressibility of the flow. However, the density of the mixture fluid was not constant. The change of the mixture fluid density was caused by the change of the mass fractions of the species within the mixture fluid. The density of the mixture fluid was determined using the volume-weighted-mixing-law [39] for the different mass fractions of the species as,

$$\rho = \frac{1}{\sum_i \frac{Y_i}{\rho_i}} \tag{5.23}$$

Where Y_i and ρ_i are the mass fraction and the density of the species i in the mixture. Other fluid properties including specific heat, thermal conductivity, and the viscosity of the mixture were also changed during the process, and were determined using the mass-weighted-mixing-law, which is based on the mass fraction average of each individual species and can be written as [39]. For the specific heat of the mixture,

$$C_p = \sum_i Y_i C_{p,i} \tag{5.24}$$

Where $C_{p,i}$ is the specific heat for species i in the mixture.

For the thermal conductivity of the mixture,

$$k_f = \sum_i Y_i k_i \tag{5.25}$$

Where k_i is the thermal conductivity for species i in the mixture.

Finally, for the viscosity of the mixture,

$$\mu = \sum_i Y_i \mu_i \tag{5.26}$$

Where μ_i is the viscosity for species i in the mixture.

5.3 CFD Model and Setup

For the setup of this validation case, the reactor was modeled as a 2-D domain using Pointwise, and the governing equations were solved using ANSYS-FLUENT 15.0. The properties of the model are listed in Table 3.

5.3.1 Boundary condition

The simulated fixed bed reactor domain is shown in Figure 10, and has a length of 0.2 m and a width of 0.127 m. The system was fed with syngas (a mixture of CO and H_2) from the inlet, and the syngas was preheated to the desired temperature before being introduced into the system. For the domain boundaries, a mass flow rate boundary condition was used at the inlet to maintain a constant gas input mass flow rate. In addition, both the top and the bottom boundaries were set as zero thickness walls and isothermally maintained at a constant temperature, and the outlet boundary condition was set as pressure outlet to keep the pressure constant in the reactor. The domain was set as a continuum of catalyst to simulate the effect of the packed bed with catalyst pellets, and all of the reactions that occurred in this domain were volumetric.

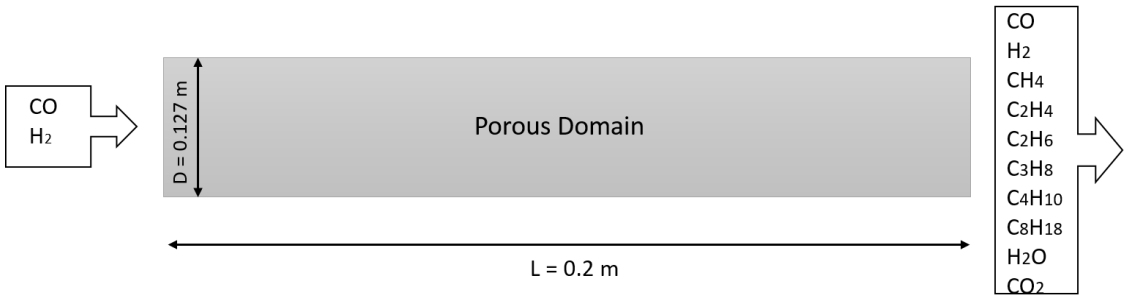

Figure 10. Reactor Domain

5.3.2 Mesh and Residuals Tolerance Independence Tests

In order to check the independence of the simulation solution on the grid, a mesh and residuals tolerance independence study was done. For this independence study, four meshes were developed, and each mesh was simulated with three different convergence criterions for the residuals tolerance. The convergence criterions were determined with the residual value of the calculated variables, for example, the mass fraction of the species, velocity, energy, and others. Detailed information about the meshes developed and the different values of the residuals tolerance tested can be found in Table 2. The conversion rate of the CO was selected as the variable to determine whether the solution was independent of the mesh and residuals tolerance or if further improvement was needed. The conversion rate of the CO was calculated as,

$$X_{\mathrm{CO}} = \frac{[\mathrm{CO}]_{in} - [\mathrm{CO}]_{out}}{[\mathrm{CO}]_{in}} \; x \; 100\% \tag{5.27}$$

Where X_{CO} is the CO conversion rates, and [CO] represents the mole concentration of CO in the reactor.

As seen from Table 2, a higher conversion rate was the result of the coarse mesh with high tolerance. Within the same mesh, as the values of the residuals tolerance began to decrease, the difference between the CO conversion rates decreased. The situation was determined to stable when the value of the residuals tolerance was set at 10^{-6}. This same observation was seen for the different meshes; as the number of elements increased in the mesh, the difference between the conversion rates decreased and eventually vanished as the mesh size was refined from 8000 elements to 15000 elements. A mesh size of 8000 elements was selected for the simulation instead

of the mesh size of 15000 elements to save computation time. Furthermore, the solution was considered to be converged when the residual of the calculated variables valued below 10^{-6}.

Table 2. Meshes and Tolerance Independent Tests for Reported Model

No. of elements	**Residuals Tolerance**	**X_{CO} (%)**
	10^{-2}	64
1500	10^{-4}	62.9
	10^{-6}	62.9
	10^{-2}	62.2
3750	10^{-4}	63.7
	10^{-6}	63.7
	10^{-2}	64
8000	10^{-4}	63.6
	10^{-6}	63.6
	10^{-2}	63.9
15000	10^{-4}	63.6
	10^{-6}	63.6

5.3.3 Simulation Setup

The SIMPLE scheme was used to couple the velocity and the pressure, and the second order upwind method was used to solve the momentum and energy equations [49]. After the energy equation was solved, data including temperature, pressure, and the mass fraction of the species were extracted and used to edit the chemical reaction rates through the UDF created for the chemical kinetic equations. Three different UDFs were developed for this simulation to calculate the following values for each grid cell throughout the domain:

1. Inlet mass flow rate
2. Reaction rates for each kinetic reaction equation
3. Fluid properties

Table 3. Parameter's Values for Reported Case [3]

Properties	**Values**
Reactor Dimension	0.2 X 0.00127 [m]
Molar Ratio of Syngas (H_2/CO)	1
Feed Temperature	563.15 [K]
Reactor Pressure	1700 [kPa]
GHSV	3000 [hr^{-1}]
Bed Porosity	0.4
Number of Tubes	1

In this FTS simulation, the species involved in the reactions are: CO, H_2, CH_4, C_2H_4, C_2H_6, C_3H_8, n_C_4H_{10}, i_C_4H_{10}, C_8H_{18}, CO_2, and H_2O. The leading FTS reactions obtained from the literature are listed below [3]:

$$\mathbf{CO + 3H_2 \xrightarrow{R_1} CH_4 + H_2O}$$

$$\mathbf{2CO + 4H_2 \xrightarrow{R_2} C_2H_4 + 2H_2O}$$

$$\mathbf{2CO + 5H_2 \xrightarrow{R_3} C_2H_6 + 2H_2O}$$

$$\mathbf{3CO + 7H_2 \xrightarrow{R_4} C_3H_8 + 3H_2O}$$

$$\mathbf{4CO + 9H_2 \xrightarrow{R_5} n\_C_4H_{10} + 4H_2O}$$

$$\mathbf{4CO + 9H_2 \xrightarrow{R_6} i\_C_4H_{10} + 4H_2O}$$

$$\mathbf{8CO + 17H_2 \xrightarrow{R_7} C_8H_{18} + 8H_2O}$$

$$\mathbf{CO + H_2O \xleftrightarrow{R_8} CO_2 + H_2}$$

The reaction rates, *R*, were given in the literature [3] as follows, and the kinetic parameters were obtained from the literature and are listed in Table 4,

$$R_i\left(\frac{mol}{hr\ g_{cat}}\right) = A \exp\left(\frac{E_i}{R_g T}\right) P_{\mathrm{CO}}^{m} P_{\mathrm{H_2}}^{n} \tag{5.28}$$

Where R_i is the reaction rate for different reactions, A is the pre-exponential value, E_i is the reaction activation energy, R_g is the universal gas constant, and m and n are the powers that the partial pressures of CO and H_2 are raised to.

Table 4. Kinetic Parameters for Reported Model Reaction Rates [3]

Reaction Number	$\boldsymbol{m}$	$\boldsymbol{n}$	$\boldsymbol{A}$	$\boldsymbol{E_i}$
1	-1.0889	1.5662	142583.8	83423.9
2	0.7622	0.0728	51.556	65018
3	-0.5645	1.3155	24.717	49782
4	0.4051	0.6635	0.4632	34885.5
5	0.4728	1.1389	0.00474	27728.9
6	0.8204	0.5026	0.00832	25730.1
7	0.5850	0.5982	0.02316	23564.3
8	0.5742	0.710	410.667	58826.3

5.4 Results

The model simulated in ANSYS-FLUENT was validated by comparing these results with the results reported in the literature [3]. In Figure 11, the molar concentration contour plots for the domain is shown for the reactants, and in Figure 12, the molar concentration contour plots for some products are also shown. For each plot, the concentration contour resulting from the ANSYS-FLUENT simulation is compared side by side with the contour obtained from the literature [3]. As can be seen in Figure 11 and Figure 12, the species concentration contours are similar for both simulations.

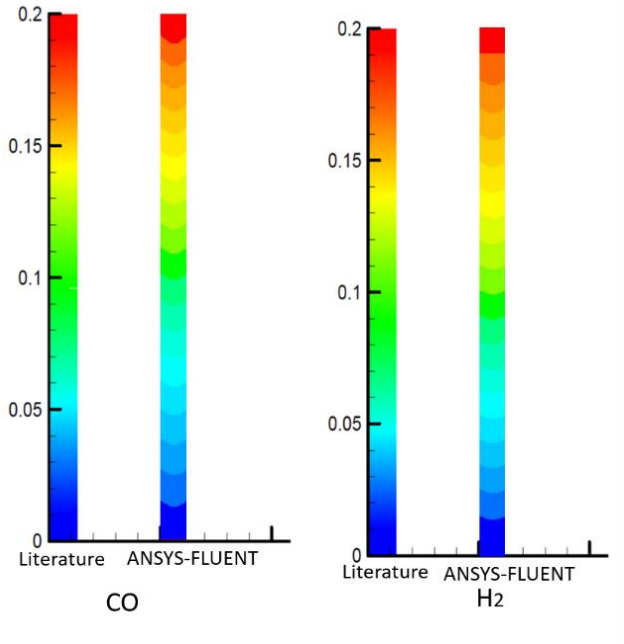

Figure 11. Molar Concentration Contours for The Reactants (X axis: width, Y axis: length)

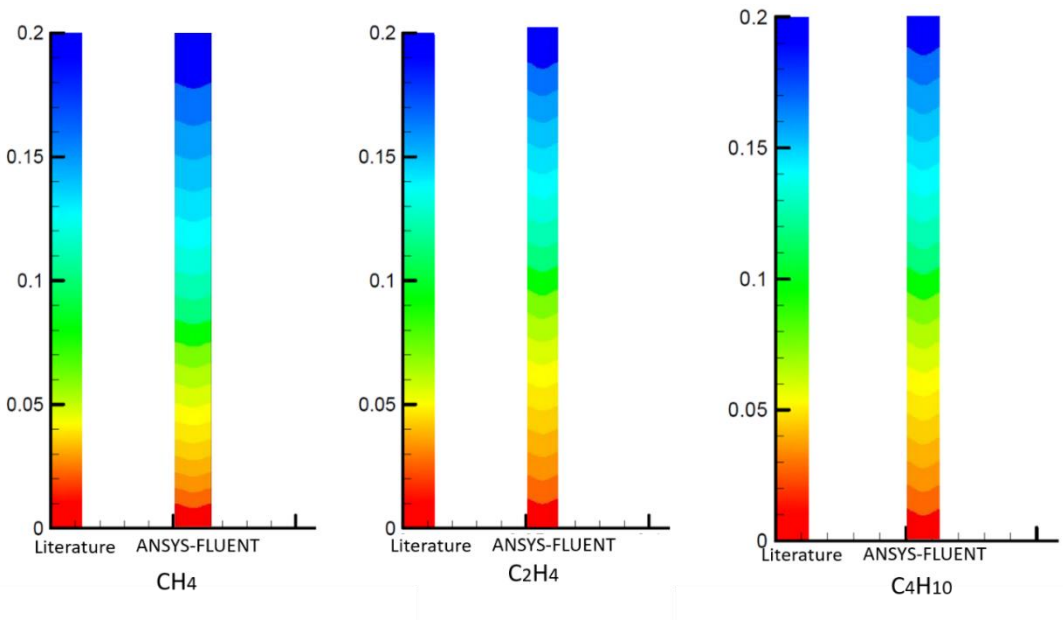

Figure 12. Molar Concentration Contours for The Products (X axis: width, Y axis: length)

The conversion rates of the reactants are also reported and compared. The species conversion rates of a system can be calculated by,

CO conversion rate,

$$X_{\mathrm{CO}} = \frac{[\mathrm{CO}]_{in} - [\mathrm{CO}]_{out}}{[\mathrm{CO}]_{in}} \; x \; 100\% \tag{5.29}$$

H_2 conversion rate,

$$X_{\mathrm{H_2}} = \frac{[\mathrm{H_2}]_{in} - [\mathrm{H_2}]_{out}}{[\mathrm{H_2}]_{in}} \; x \; 100\% \tag{5.30}$$

And syngas conversation rate,

$$X_{\mathrm{CO+H_2}} = \frac{[\mathrm{CO+H_2}]_{in} - [\mathrm{CO+H_2}]_{out}}{[\mathrm{CO+H_2}]_{in}} \; x \; 100\% \tag{5.31}$$

Where X is the species conversion rates, $[i]$ represents the mole concentration of that species, and i is the species.

Table 5 lists the conversion rates of CO, H_2, and syngas from the reported results [3] and also the results from the ANSYS-FLUENT simulation.

Table 5. Reported Results Compared with ANSYS-FLUENT Results

Conversion Rate	**Model reported** [3]	**ANSYS-FLUENT Model**	**Relative Error [%]**
X_{CO} (%)	70.1	64.5	7.9
X_{H_2} (%)	59	49	16.9
X_{H_2+CO} (%)	64.5	57.2	11.3

For the conversion rate of CO, the ANSYS-FLUENT model showed a relative error within 10% with the reported model, which is acceptable. However, for the H_2 conversion rate, the error between the ANSYS-FLUENT model and the reported model is relatively large. This is most likely due to the limitation of how ANSYS-FLUENT can define the stoichiometry of the chemical reaction. Reaction 7 is presented in the literature as,

$$8.96CO + 18.05H_2 \xrightarrow{R_7} C_{8.96}H_{18.18} + 8.96H_2O \tag{5.32}$$

but for ANSYS-FLUENT, only a whole number can be used to define the stoichiometry of the reaction. Therefore, whereas this reaction uses 18.05 H_2 molecules, in the ANSYS-FLUENT simulation, only 17 H_2 molecules can be used so as to maintain the balance of the chemical equation. Because the reaction rate of the two models stayed the same, the conversion rate of H_2 was less in the ANSYS-FLUENT simulation compared to the H_2 conversion rate reported in the literature.

5.5 Summary

In this section, the reported FTS system model simulated by employing the finite volume method was re-produced using ANSYS-FLUENT. The results from both simulations were reported in order to validate the use of ANSYS-FLUENT for the FTS system simulation.

Instead of simulating a domain with catalyst pellets modeled inside the reactor, a continuum of catalyst was used to represent the reactor with a packed catalyst bed. The detailed model of the porous media was discussed. Also, for the FTS system, the main fluid was a fluid mixed with different species; therefore, the fluid properties equations for the main fluid needed to be modified to incorporate the involved species. The modified equations were discussed in this section.

Finally, for the reactor model, a 2-D domain with a length of 0.2 m and width of 0.127m was created using Pointwise. The mashed domain was imported into ANSYS-FLUENT, and boundary conditions were applied to the domain. A mesh and residuals tolerance independent test was performed to determine the effect the grid size and the residuals tolerance had on the CO conversion rate. A mesh size and a value for the convergence criterion of the residuals tolerance were selected for the simulation. Three UDFs were created in ANSYS-FLUENT to calculate the inlet mass flow rate, the reaction rates, and the fluid properties for the simulation. At the end of this section, the reported results from the literature for the species molar concentration contour plots and the conversion rate for the reactant gas were compared to the results obtained from ANSYS-FLUENT. The comparison of the reactants conversion rate and the species molar concentration contour showed an acceptable agreement between the two models.

CHAPTER 6

SIMULATION OF FTS MODEL WITH PID CONTROLLER

Chapter 5 validated the model from the literature. This Chapter presents the ANSYS-FLUENT model developed for this dissertation. The details of the reactor model, the development of the kinetic model for the reaction, the condition of the simulation, and the methodology are discussed in this section.

6.1 Detailed Reactor Model

In this section, for the fixed-bed reactor model, a 2-D pseudo-homogeneous model was developed with a 2-D axisymmetric domain. The dimensions of the region had the width of 0.002 m and the length of 0.53 m.

6.1.1 Boundary Conditions

After the domain was created, it was imported into the ANSYS-FLUENT software for simulation. Syngas was fed into the system inlet from the left boundary, which was set as the mass flow rate boundary condition as shown in the Figure 13. The top boundary of the domain was set as a wall with zero thickness and heated isothermally. In addition, the bottom boundary was set as insulated because it was designed to be the center axis for the domain to rotate about and create a 3-D domain. The boundary on the right was set as a pressure outlet. The pressure of the system was defined on this boundary and was maintained constant during the simulation.

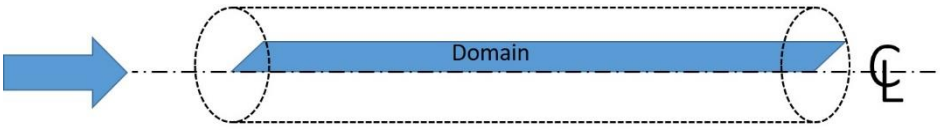

Figure 13. Reactor Model

6.2 FTS Reaction Kinetic Model

For FTS, the kinetic model is obtained from the reaction rate expressions and the products distribution of the system. A kinetic model based on experiments done by other researchers found in the literature was used in Chapter 5; however, no literature was found that had the same experimental system setup as used in this dissertation. Therefore, in this section, the development of the kinetic model for the chemical reactions presented in this dissertation is presented.

A FTS kinetic model is used to describe the transformation of the reactants to products [50]. From the long history of FTS, many studies were done with this process, and the kinetic model for FTS can be summarized into two reactions:

1. The main reaction for products (a forward reaction).
2. The water-gas shift reaction (a reversible reaction).

The main reaction describes on a molecular level the transformation of the reactant, the syngas, to the products, which are hydrocarbon products and water in this case. From literature, the simple overall summary reaction can be written as [51]:

$$(2n+1)\mathrm{H_2} + n\mathrm{CO} \xrightarrow{\mathrm{R}} \mathrm{C_nH_{(2n+2)}} + \mathrm{H_2O} \tag{6.1}$$

Where n is the number of moles, and R is the reaction rate.

In addition, the water-gas shift reaction is:

$$CO + H_2O \overset{R_W}{\leftrightarrow} CO_2 + H_2 \quad (6.2)$$

The water-gas shift (WGS) reaction is a reversible reaction and is usually find to be at equilibrium throughout the entire process [52]. However, for the Co based catalyst used in this study, the WGS reaction is either very limited or does not occurred in the process [12, 14], therefore, the WGS reaction is disregarded.

In order to have a kinetic model that can usefully describe the FTS system, it must have the following features [53, 54]:

1. The carbon number of the products accounted for must be sufficiently high, for example C_{20+}, because these high carbon number products are important for the production of liquid fuel.
2. The trends of the activity and the selectivity for the kinetic model with the process conditions should reflect the same trends expected from the experiment data.
3. During the FTS process, more than 99 mol% of the reacting species are in gas phase; therefore, the flowing phase in the reactor can be assumed to be entirely gas, and the liquid flow is ignored.

6.2.1 FTS syngas consumption rate expression literature review

The reaction of FTS is defined by the reaction rate. Over the years, the reaction kinetics of FTS have been well studied. In most literature, power law models are commonly used to describe the reaction kinetics of FTS. These empirical models require fitting experimental data into a nonlinear regression model. In more recent studies, the Hougen-Watson model is widely used for the reaction kinetics of FTS, and the model has the form [55],

$$rate = \hat{y} = \frac{\beta_1 \cdot x_2 - x_3/\beta_5}{1+\beta_2+x_1+\beta_3+x_2+\beta_4 \cdot x_3} \tag{6.3}$$

Where $\beta_1 \cdots \beta_5$ are unknown parameters, and x_1, x_2, x_3 are input variables.

While Hougen-Watson model is generally a purely empirical power law model without any theoretical significance, Froment used this model to systemically account for the interactions of the reacting species with the catalyst [56].

From experiments, the FTS reaction rate, or the rate of the syngas being consumed to product products in the system, is well known for its dependence on the partial pressure of H_2 in the form,

$$R_{FT} = k_1 P_{\mathrm{H_2}} \tag{6.4}$$

Where R_{FT} is the rate of syngas being consumed, k_1 is the rate constant determined by the experiment. In the study by Anderson et al., they had found that the rate equations with the dependence on the partial pressure of H_2 was acceptable for an FTS system with a syngas conversion rate up to 60% [57]. The activation energy from the reaction was found to be in the rage of 80 - 88 kJ/mol, depending on the type of catalyst [57]. At higher conversion rates, rate inhibition can occur in the system. Therefore, Anderson et al. proposed an alternative rate equation for the system with a conversion rate higher than 60%, which includes the effect of water,

$$R_{FT} = \frac{k_0 P_{\mathrm{CO}} P_{\mathrm{H_2}}}{P_{\mathrm{CO}} + a P_{\mathrm{H_2O}}} \tag{6.5}$$

Where a is an adsorption term.

Atwood and Bennett used the equation (6.5) to calculate the reaction rate for their fused, nitride ammonia synthesis catalyst and found that the effect of water only occurred at the highest temperature and conversion rate. They determined the activation energy to be 85 kJ/mol and the adsorption term to be -9 kJ/mol in their system [58].

Huff and Satterfield also did a study using the equation (6.5) on their fused iron ammonia synthesis catalyst and found that the adsorption term decreased linearly with the partial pressure of H_2 [59]. In order to account for this dependence, Huff and Satterfield derived an alternative rate equation for the FTS system,

$$R_{FT} = \frac{k_0 P_{\mathrm{CO}} P_{\mathrm{H_2}}^2}{P_{\mathrm{CO}} P_{\mathrm{H_2}} + b P_{\mathrm{H_2O}}} \tag{6.6}$$

To better fit data into this model, Huff and Satterfield included an additional constant term in the denominator from Anderson's rate equation, and they found that the activation energy for their FTS system to be 83 kJ/mol.

Philippe et al. developed an FTS simulation with a 2-D pseudo-homogeneous steady-state plug flow model to study the structural and thermal properties of an FTS cobalt-based catalyst in a fixed bed [60]. For the kinetic rate expressions of their model, Philippe et al. based their simulation on the expressions reported by van der Laan as [61],

$$R_{FT} = \frac{A_a \cdot \exp(\frac{-E_a}{R_g T})[\mathrm{CO}][\mathrm{H_2}]}{(1 + A_b \cdot \exp(\frac{-E_b}{R_g T})[\mathrm{CO}])^2} \tag{6.7}$$

Where [CO] and [H_2] are the concentrations of the species, E is the activation energy, A_a, A_b, A_C are pre-exponential factors, and R_g is the universal gas constant. Using this expression, they were able to reach a reasonable agreement between the simulation results and the experimental

data of the heat released from the system. In this expression, instead of using the partial pressure to determine the FTS reaction rate, the concentrations of the reactants were considered, along with two constants that were adjusted to better fit the expression with the experimental data. Using this expression, the activation rate they found was about 100 kJ/mol.

Some conclusions can be drawn from observations of the above studies. (1) The activation energy for the FTS system was about 80-100 kJ/mol, disregarding the type of catalyst. Huff and Satterfield reviewed a larger range of studies and found that the activation energy for FTS ranged from 65 kJ/mol to 105 kJ/mol [53]. (2) At conversion rates lower than 60%, all of the reported rate expressions of FTS were reduced to first order dependence of H_2 molar concentration in the system.

6.2.2 FTS products formation rate expression literature review

Similar with the FTS syngas reaction rate, the development of the products formation rate can also employ the empirical power law and the Hougen-Watson model. The power law is useful for expressing the syngas reaction rate as it has simplicity in form, but for use for the products formation rate, there is a disadvantage. One power law must be used to represent the formation of one product, and from previous studies, at least two or more constants need to be determined for each power law. Due to the large amount of products formed in an FTS reaction, a large number of constants must be obtained to completely describe the FTS kinetic model. For this reason, the power law model is usually only used for lower carbon number products. For the heavier products, or products with higher carbon number, an assumed distribution like Schulz-Flory distribution is used [53].

Zein el Denn et al. has found the reaction rate expression for C_1-C_4 as [62],

$$R_j = k_j P_{CO}^{n_j} P_{H_2} \tag{6.8}$$

Where R_j is the reaction rate of species j, and n_j is a constant.

For products higher than C_5, a Schulz-Flory distribution was used, and the rate was expressed with the relation to CO reaction rates as,

$$R_c = \beta_0 \alpha^c (-R_{CO}) \tag{6.9}$$

Where β_0 is a constant, and c is the carbon number. The value of α and β_0 can be obtained from the Schulz-Flory plot of the data. In their experiment, they found that the activation energy for formation of C_1-C_4 products was about 105-135kJ/mol.

Bub and Baerns studied a similar system but for the formation of lower carbon number products. They added an additional exponent to the H_2 partial pressure [63],

$$R_j = k_j P_{CO}^{n_j} P_{H_2}^{m_j} \tag{6.10}$$

They also used the approach with the Schulz-Flory distribution for products with a carbon number higher than 5. They found the activation energy for formation of C_1-C_4 products to be in the range of 94-126 kJ/mol.

In addition, Kellner and Bell studied the FTS system using the same approach as Bub and Baerns to determine the formation rate for methane in an FTS system [64]. However, in their study, they did not consider the formation of CO_2 in the water gas shift reaction. They reported the methane formation rate as,

$$R_{CH_4} = k_4 P_{CO}^{-1} P_{H_2}^{1.5} \tag{6.11}$$

Moreover, the activation energy they found for the formation of methane was 117 kJ/mol. The Schulz-Flory distribution was also used to determine the formation rate of the higher carbon number products.

Van der Laan reported an expression for the methane formation rate using the concentration of the reactants. His expression is simply related to the syngas reaction rate by the Arrhenius law [61],

$$R_{CH_4} = A_c \cdot \exp(\frac{-E_c}{R_g T}) R_{FT} \tag{6.12}$$

The activation energy he obtained from methane formation of his system was 81 kJ/mol.

Some conclusions can be drawn from this literature review. (1) The power law model is simple in form, but it has its limitation. One power law model is needed for each product. Because the FTS system produces many different products, a large amount of constants need to be obtained in order to completely describe the FTS kinetic model. (2) Schulz-Flory distribution can be used to extrapolate the products with a higher carbon number. A reasonable agreement between the Schulz-Flory distribution and the distribution of products was observed in the literature.

6.2.3 Experiment Data

For the FTS process, the data was obtained from conducting experiments with two different system temperatures of 528 K and 543 K. The products of FTS were analyzed in gas chromatographs (GC). The liquid products were analyzed in the GC (SRI 8610) with a Restek MXT-500 SimDist capillary column. Also, the gas products were analyzed in the GC (SRI

8610C) with a Shin Carbon ST 80/100 column and Thermal conductivity detector (TCD). Figure 14 shows the amount of products created in the process in one experiment.

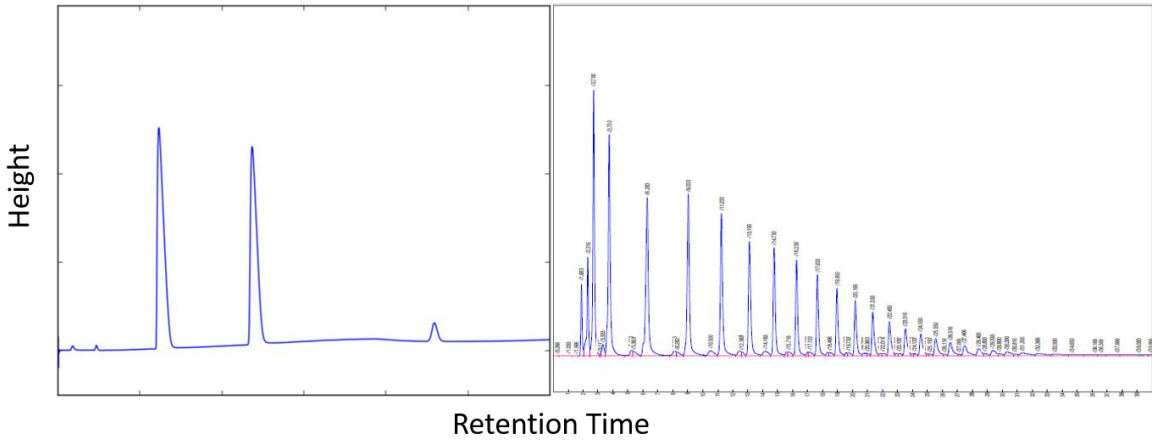

Figure 14. Sample of Gas Chromatograph Results (Left: Gas, Right: Liquid)

In order to ensure the repeatability of these experiments, three experiments were completed at each system temperature. In addition, the resultant data for each system temperature were obtained by averaging the three experimental data. The resulted averages and the experiment data were shown in Table 6, and the unit was in mol/hr.

Table 6. Experiment Data

	CH_4	$C_{14}H_{30}$	$C_{25}H_{52}$		CH_4	$C_{14}H_{30}$	$C_{25}H_{52}$
	0.015013	0.000388	0		0.052218	0.00021157	0
T=528 K	0.016887	0.000239	0	T=543 K	0.040189	0	0
	0.012853	0.000464	3.03E-06		0.012313	0.00020735	9.23E-06
Average	0.014918	0.000363	1.01E-06	**Average**	0.034906	0.00013964	3.08E-06
SD	0.002019	0.000114	N/A	**SD**	0.02047	2.9824E-06	N/A

Using the experimental data, the chemical equations with their specific reaction rates were found. Due to the large number of the hydrocarbon products resulting from the experiment (C_1 to C_{28}), they were combined into the following components:

1. Gas (C_1 to C_4)
2. Light Oil (C_5 to C_{24})
3. Wax (C_{25} to C_{28})

Furthermore, in each component, a chemical equation was adopted to represent that component.

A weighted average was used within each component in order to determine a chemical equation suitable for that component, with the assumption that each of the reaction rate constants was a function of all the carbon numbers in the same component. The resulting chemical equations used for the corresponding components are:

1. Gas

$$12H_2 + 4CO \rightarrow 4CH_4 + 4H_2O \tag{6.13}$$

2. Light Oil

$$29H_2 + 14CO \rightarrow C_{14}H_{30} + 14H_2O \tag{6.14}$$

3. Wax

$$51H_2 + 25CO \rightarrow C_{25}H_{52} + 25H_2O \tag{6.15}$$

From the chemical equations above, the reaction rates for each equation need to be defined. The reaction rates determine the rate of production of hydrocarbon products in the system. The

methodology for defining the reaction rates for each chemical equation is discussed in the following section.

6.2.4 Gas

In this dissertation, methane was used to represent the gas products formation in FTS reaction. For the methane production of FTS, work of many groups was studied and it was found that, the formation rate of methane can be defined by an expression that obey the Arrhenius law,

$$R_{CH_4} = A_c \cdot \exp(\frac{-E_c}{R_g T}) R_{FT} \tag{6.16}$$

where E_c is the activation energy and A_c is the pre-exponential factor. The activation energy of the reaction, represents the level of energy needed for the reaction to start, this value is determined by interpretation of the data from the experiment. The pre-exponential factor represents the total number of molecular collusions happening in the system for a given time period, this value can be found by plotting the relationship between the logarithm of the reaction rate and its corresponding inverse of temperature.

To obtain the activation energy values and the pre-exponential factor of the Arrhenius law, Hooke and Jeeves had proposed a direct search method and found to be very successful on obtaining those constants [65]. But in this thesis, due to the lack of experimental data, the use of any non-linear regression algorithms to determine the all of the unknown variables become impossible. Therefore, the values for the formation rate of CH_4 was obtain from the studies contained in the previous literature review section. From the review, the expression reported by Philippe was selected to be used in this dissertation. This is because the system conditions they reported in their research were the closest to the conditions used in this dissertation. The rate was expressed as,

$$\frac{\partial[CH_4]}{\partial t} = R_{CH_4} = A_c \cdot \exp(\frac{-E_c}{R_g T}) R_{FT} \quad (6.17)$$

and,

$$R_{FT} = \frac{A_a \cdot \exp(\frac{-E_a}{RT})[CO][H_2]}{(1+A_b \cdot \exp(\frac{-E_b}{R_g T})[CO])^2} \quad (6.18)$$

The values for the variables for the methane formation rate are listed in Table 7,

Table 7. Values for Methane Formation Rate

Variables	**Values**
E_a	100 [kJ/mol]
A_a	3.42 [m^6/mol/g/s]
E_b	20 [kJ/mol]
A_b	0.45 [m^6/mol/g/s]
E_c	81 [kJ/mol]
A_c	1.94 [m^6/mol/g/s]
R_g	0.008314 [kJ/mol-k]

6.2.5 Light Oil and Wax

For the higher carbon number components, less literature was found discussing heavy hydrocarbon products (C_{10+}). Moreover, as stated earlier, power law models are limited to lower

carbon number models. Therefore, in order to extrapolate to the higher carbon number components, an assumed distribution model, the Anderson-Schulz-Flory (ASF) distribution is more suitable [51, 66]. By using the ASF distribution, the reaction rate can be determined with the chain growth probability and the consumption rate of the CO gas,

$$R_c = \alpha^c \beta(-R_{\mathrm{CO}}) \tag{6.19}$$

Where c is the carbon number, α is the chain growth probability, β is a constant, and $-R_{\mathrm{CO}}$ is the consumption rate of the CO gas.

ASF distribution can be used to predict the chain growth probability of the hydrocarbon chain from experimental data [66]. By using the ASF distribution, the hydrocarbon chain in the FTS reaction is assumed to be formed step-wise by adding a one-carbon molecule to the chain at a time, and the ASF distribution determines the probability of the chain to grow to a defined length [66]. The ASF distribution may be derived as follows,

$$\ln \frac{W_c}{c} = c \ln \alpha + \mathrm{Const.} \tag{6.20}$$

Where W_c is the mass fraction for the species with carbon number c, and α is the chain growth probability. By plotting ln (W_c/c) against c for different temperatures as shown in Figure 15, the chain growth probability can be evaluate from the slope of the plot [12, 51].

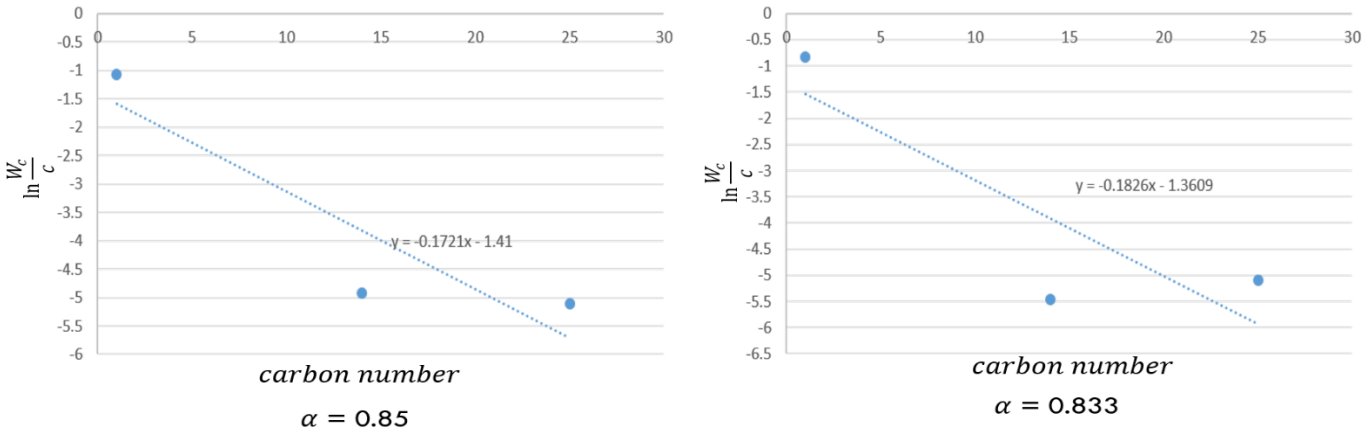

Figure 15. ASF Distribution Plot (Left: T = 528 K, Right: T = 543 K)

Figure 16 shows the chain growth probability α in the FTS with different temperatures. Using this plot, a function for α with respect for temperature can be obtained as,

$$\alpha(T) = -0.0011T + 1.445 \tag{6.21}$$

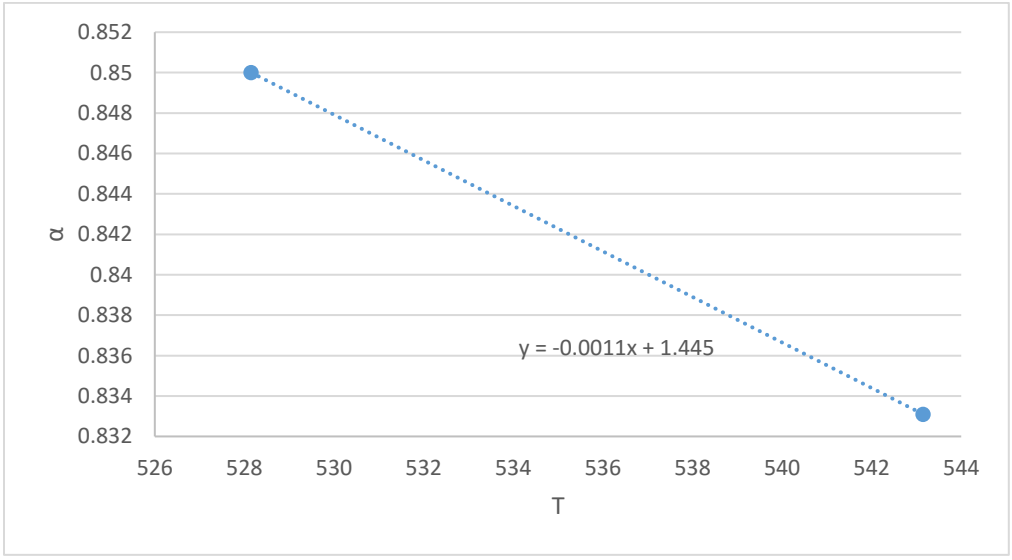

Figure 16. Chain Growth Probability VS. Temperature

and the consumption rate of the CO gas can be found by in the literature [67] as,

$$\frac{\partial[\mathrm{CO}]}{\partial \mathrm{t}} = R_{\mathrm{CO}} = 1.64\mathrm{e}5 \exp\left(\frac{-105}{R_g T}\right) P_{\mathrm{H_2}}^{1.1} P_{\mathrm{CO}}^{-0.2} \tag{6.22}$$

With all the variables obtained, the complete FTS kinetic model used in this dissertation is shown in Table 7,

Table 7. FTS Kinetic Model

Chemical equations:
$12H_2 + 4CO \rightarrow 4CH_4 + 4H_2O$
$29H_2 + 14CO \rightarrow C_{14}H_{30} + 14H_2O$
$51H_2 + 25CO \rightarrow C_{25}H_{52} + 25H_2O$
Species formation/consumption rates:
$R_{H_2} = \frac{\partial[H_2]}{\partial t} = -\frac{3.42\exp\left(\frac{-100}{0.008314T}\right)[CO][H_2]}{\left(1+0.45\exp\left(\frac{-20}{0.008314T}\right)[CO]\right)^2} - \sum_{i=1}^{N}(i+1)\cdot R_{C_i}$ Where R_{C_i} is the formation rate of product with carbon number i.
$R_{CO} = \frac{\partial[CO]}{\partial t} = 1.64e5\exp(\frac{-105}{R_g T})P_{H_2}^{1.1}P_{CO}^{-0.2}$
$R_{CH_4} = \frac{\partial[CH_4]}{\partial t} = 1.94\exp(\frac{-81}{0.008314T})\frac{3.42\exp(\frac{-100}{0.008314T})[CO][H_2]}{(1+0.45\exp(\frac{-20}{0.008314T})[CO])^2}$

$$R_{C_{14}H_{30}} = \frac{\partial[C_{14}H_{30}]}{\partial t} = (-0.0011T + 1.445)^{14}(0.0424T - 22.24)[-1.64e5 \exp\left(\frac{-105}{R_g T}\right) P_{H_2}^{1.1} P_{CO}^{-0.2}]$$
$$R_{C_{25}H_{52}} = \frac{\partial[C_{25}H_{52}]}{\partial t} = (-0.0011T + 1.445)^{25}(0.0058T - 3.0769)[-1.64e5 \exp\left(\frac{-105}{R_g T}\right) P_{H_2}^{1.1} P_{CO}^{-0.2}]$$
$$R_{H_2O} = \frac{\partial[H_2O]}{\partial t} = \frac{\partial[CH_4]}{\partial t} + 14\frac{\partial[C_{14}H_{30}]}{\partial t} + 25\frac{\partial[C_{25}H_{52}]}{\partial t}$$

After the reaction rates were found, the kinetic model for this FTS was completed and readied to be simulated in ANSYS-FLUENT. In the next section, the setup in ANSYS-FLUENT is discussed.

6.3 ANSYS-FLUENT Methodology

Most of the settings for ANSYS-FLUENT were similar to those used in Chapter 5 except for the setting of the diffusion coefficients. The conditions used for this simulation are shown in Table 8,

Table 8. FTS Simulation Conditions

Properties	**Values**
Molar Ratio of Syngas (H_2:CO)	2:1
Set-point Temperature	522 [K]
Reactor Pressure	2068 [kPa]
Gas Hourly Space Velocity (GHSV)	900 & 2702 [hr^{-1}]
Number of Tubes	1

The gas hourly space velocity (GHSV) is defined as,

$$GHSV = \frac{Reactant\ Gas\ Flow\ Rate}{Reactor\ Volume} \tag{6.23}$$

For the validation simulation, the values of the molecule specific parameters for the products were either recorded in the database of ANSYS-FLUENT or were found in the literature. Therefore, a kinetic theory can be used to obtain the diffusion coefficients for the validation simulation to use. However, in this simulation, the molecule specific parameters for the products $C_{14}H_{30}$ and $C_{25}H_{52}$ were neither recorded in any database nor found in the literature, so a different approach had to be used for the calculation of the diffusion coefficients. A binary diffusion equation for the gas-phase was used to obtain the diffusion coefficients [68],

$$D_{AB} = \frac{0.001T^{1.75}[(M_A+M_B)/(M_AM_B)]^{1/2}}{P[(\sum V)_A{}^{1/3}+(\sum V)_B{}^{1/3}]^2} \quad (6.24)$$

where D_{AB} is the diffusion coefficient between species A and B, M_A and M_B are the molecular weights, and $\sum V$ is the sum of diffusion volumes of the species. For the species used in this dissertation, the sum of diffusion volumes was calculated and is shown in Table 9,

Table 9. Diffusion Volumes

Species	$\sum V$ **[pm^3]**
CO	18.9
H_2O	12.7
$C_{14}H_{30}$	290.4
CH_4	24.42
$C_{25}H_{52}$	515.46
H_2	7.07

In addition to the UDFs used in the previous simulation, a new UDF was developed to calculate the diffusion coefficient between different species, and the diffusion coefficient was applied to the simulation according to the mass fraction of the mixture.

6.4 Mesh and Residuals Tolerance Independence Tests

As with the model developed in the previous section, a mesh and residual tolerance independence test was also performed on this model. This test was used to determine the mesh

size and the tolerance for the residual convergence criteria in this FTS simulation. The convergence criteria were determined with the residual values of the calculated variables, for example, the mass fraction of the species, velocity, energy, and others. The results of this test are shown in Table 10. The conversion rate of the CO was selected as the variable to determine whether the solution was independent of the mesh and residuals tolerance or if further improvement was needed.

Table 10. Mesh and Residuals Tolerance Independence Tests for FTS Model

No. of elements	**Residuals Tolerance**	**X_{CO} (%)**
	10^{-2}	45
2396	10^{-3}	44
	10^{-4}	44
	10^{-2}	35
5593	10^{-3}	36
	10^{-4}	36
	10^{-2}	29
10791	10^{-3}	30
	10^{-4}	30
	10^{-2}	29
14289	10^{-3}	30

	10^{-4}	30

As observed from Table 10, a higher conversion rate resulted from the coarser mesh; as the mesh became more refined, the conversion rate decreased and stabilized at 30%. The same behavior was also observed from the different values of the residuals tolerance within the same mesh size; as the values of the residuals tolerance decreased, the difference between the CO conversion rates also decreased, and the conversion stabilized when the value of the residuals tolerance was set lower than 10^{-3}. Therefore, from this result, a domain meshed in a grid generator program Pointwise with 10791 elements was developed, and for the simulation, a value of 10^{-4} was set as the residuals tolerance for the convergence criteria.

6.5 Experiment Setup

The prepared catalyst was placed in the mid-section of the steel tube reactor. The bed height was about 3 inches and was held stable by glass wool placed at both ends of the bed to prevent the bed from shifting during the process. Syngas was fed into the reactor from the inlet at the top using the flow controller (Omega FMA 5400/5500 Mass Flow Control) to maintain the desired flow rate. The gas product from the outlet was condensed in a chamber to form liquid products that collected at the bottom of the pressure vessel. A pressure relief valve was connected to the pressure vessel and set to maintain a pressure of 300 psig inside the system. For the non-condensable gas, a flow meter (Omega FMA 4000 Digital Mass Flow Meter) was used to monitor the outlet gas flow rate of the system.

An electric furnace was used as the heating source of the system. The reactor was placed in the middle of the electric furnace controlled by a proportional-integral-derivative (PID)

controller (Omega CN 2700). The PID controller received feedback temperature from the thermocouple located inside the reactor and calculated the output temperature for the electric furnace to maintain the desired temperature in the system.

A Labview data acquisition system (NI CDAQ-9174) was used for real time data collection. The Labview system monitored the outlet flow rate and the temperature in various locations. The temperature was taken inside the reactor to determine the system temperature, and this was used as the controller feedback signal. In addition, the temperature was taken in the pressure vessel to monitor the condenser temperature, and on the inside surface of the furnace. All data was saved in the computer for further performance analysis. The settings for the experiment are listed in Table 11,

Table 11. FTS Experiment Condition Values

Properties	**Values**
Reactor Dimension	0.5 x 0.00833 [m]
Molar Ratio of Syngas (H_2/CO)	2:1
Set Point Temperature	522 [K]
Reactor Pressure	2068 [kPa]
GHSV	900 & 2702 [hr^{-1}]
Bed Porosity	0.9
Number of Tubes	1

Proportional Band	47 [%]
Integral Time	208 [rep/min]
Derivative Time	41 [min]

The parameter values in the Omega CN 2700 controller were displayed in proportional band (PB), integral time (T_i), and derivative time (T_d). However, the parameters of the PID controller developed in this dissertation were defined in gains ($k_p,\ k_i,\ k_d$). Therefore, the below equations were used to convert the parameters to PID gains [69],

$$K = \frac{100\%}{PB}$$

Where K is controller gain. The output signal is defined as,

$$u(t) = K[e(t) + \frac{1}{T_i}\int e(t)\,\mathrm{d}t + T_d\frac{\mathrm{d}e}{\mathrm{d}t}] = k_p e(t) + k_i\int e(t)\,\mathrm{d}t + k_d\frac{\mathrm{d}e}{\mathrm{d}t}$$

Therefore,

$$k_p = K$$

$$k_i = \frac{K}{T_i}$$

$$k_d = KT_d$$

In addition, the final PID gain values used in the system are listed in Table 12,

Table 12. FTS Simulation System PID Gains

Gains	Values
k_p	2.12
k_i	0.01
k_d	86.9

6.6 Results and Discussion

After the simulation was setup, it was connected with the PID controller that was previously developed in MATLAB. The MATLAB and ANSYS-FLUENT software were then compiled together with the settings used in this experiment.

One of the goals of this dissertation was to measure the performance of the PID controller when used to control a system with different heat releasing rates. Chapter 4 presents the results of adding different levels of a heat source to the tube model, which was simulated with the PID controller. The heat source added to the model was in the form of,

$$S_R = T^n \tag{6.25}$$

The results from Chapter 4 show that the system was defined as “uncontrollable with the PID controller” when the heat source added to the model was,

$$S_R = T^{1.8} \tag{6.26}$$

These results show that the PID controller can only be used to control the system with energy density (W/m^3) under a certain limit; as the energy released from the system goes beyond that limit, the PID controller has difficulty maintaining the system at the set point temperature.

To determine the controllability of the FTS model used in this dissertation, the amount of heat energy released from the system when using different inlet flow rates was obtained from the simulations. The amount of heat released from the system can be reflected by the heat density. Table 13 reports the values of the total heat flux over the model's boundaries and the heat density for both the FTS model and the tube model presented in Chapter 4.

Table 13. Heat Flux Values for the System

Case Numbers	**Conditions**	**Total Heat Flux [W]**	**Heat Density [W/m^3]**
T(1.4)	n = 1.4	1.54E+01	2.31E+06
T(1.5)	n = 1.5	7.06E+01	1.06E+07
T(1.6)	n = 1.6	1.82E+02	2.73E+07
T(1.7)	n = 1.7	4.16E+02	6.25E+07
T(1.8)	n = 1.8	1.03E+03	1.54E+08
100 SCCM	flow rate = 100 SCCM	4.28E+02	6.42E+07
300 SCCM	flow rate = 300 SCCM	5.79E+03	8.69E+08

To easily compare between the different systems, a bar plot for the total heat flux of systems is also presented,

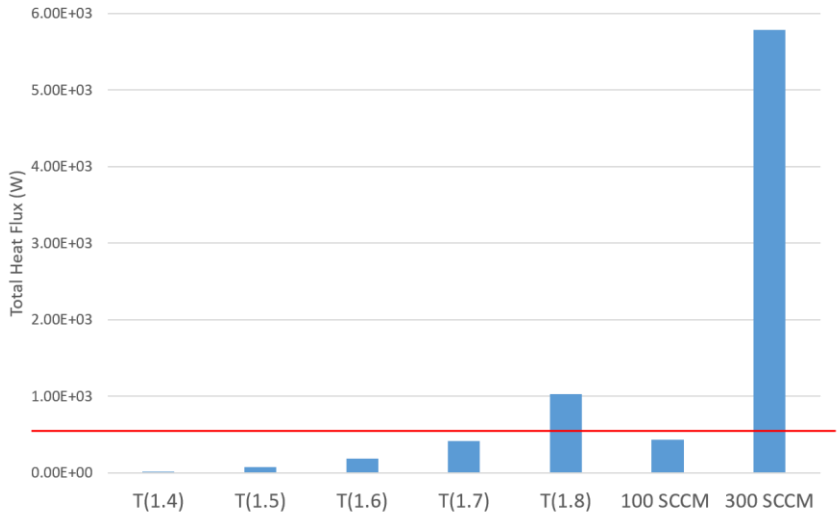

Figure 17. Total Heat Flux Value for Systems

The red line in Figure 17 represents the maximum heat flux value the PID controller can handle; systems that have values below the red line can maintain a stable system temperature, as observed in Chapter 4. Similar with the observations in Chapter 4, with the FTS model used in this chapter, the PID controller should have the ability to control the system when the inlet flow rate is lower or equal to 100 SCCM. As the flow rate increases to 300 SCCM, the heat released from the system should be too rapid for the PID controller to handle. This same observation was seen from the experimental data obtained in Chapter 3 for the experimental system when the inlet flow rate was set to 100 SCCM and 300 SCCM.

Figure 18 shows a 12 hour period of the temperature profile obtained from the experiment. Instead of showing the temperature profile of the entire process, which lasted for 92 hours, a section of the profile was selected to better show the details of the system's temperature behavior. This 12 hour time period was chosen based on its location in the middle of the experiment process

when the system had warmed up with the catalyst activated, but had not moved far enough along in the process where the catalyst had started to show any signs of deactivation.

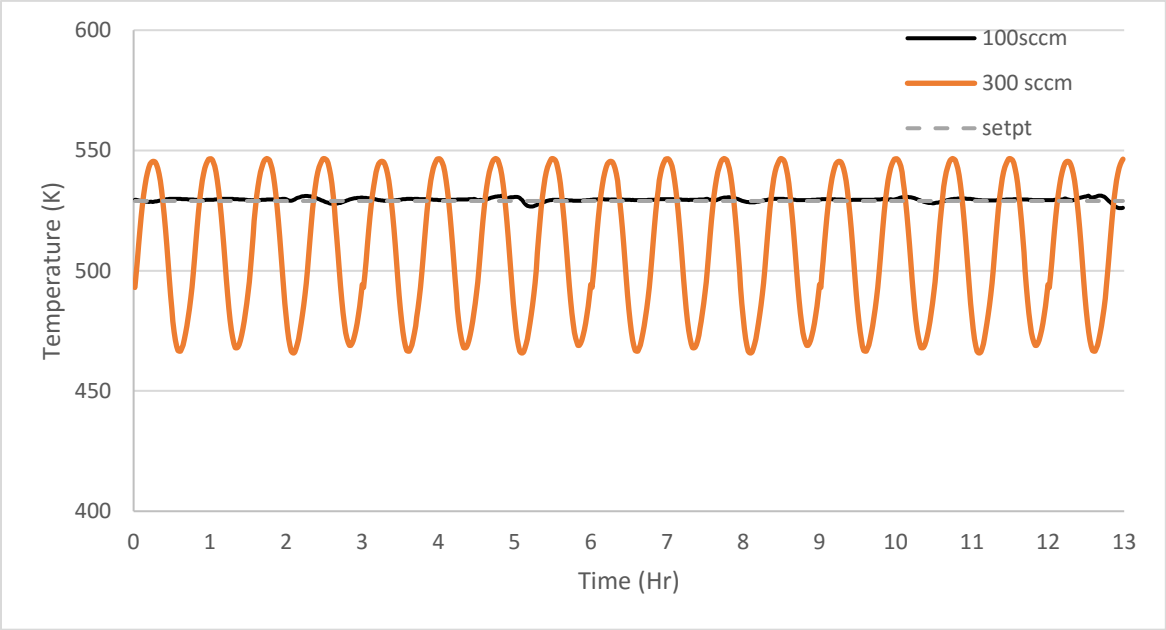

Figure 18. Temperature Profile over 12-hour period

As shown in Figure 18, the heat up and cool down frequency was consistent during the experiment. The simulation studied in this dissertation intends to develop a complete system, including the reactor simulation and the control system, which is able to repeat the behavior of the experiment, so any further study can be done using this method developed.

A 100 SCCM inlet flow rate system was simulated with the PID controller. After the data was collected and processed, a plot of the simulated system temperature was created, which is shown in Figure 19, and a plot of PID controller output temperature was shown in Figure 20. In order to implement this PID controller into the real system setup, the PID controller output temperature was limited to the range of 300 K to 800 K, in which 300 K was the room temperature and 800 K was the maximum temperature the furnace can output.

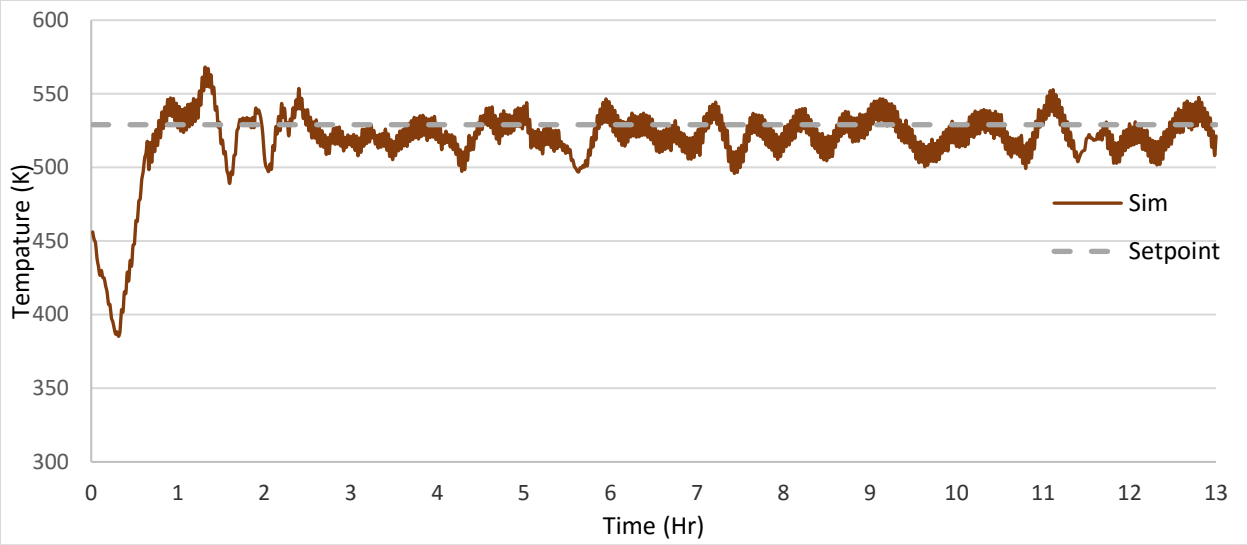

Figure 19. 100 SCCM Simulation Results

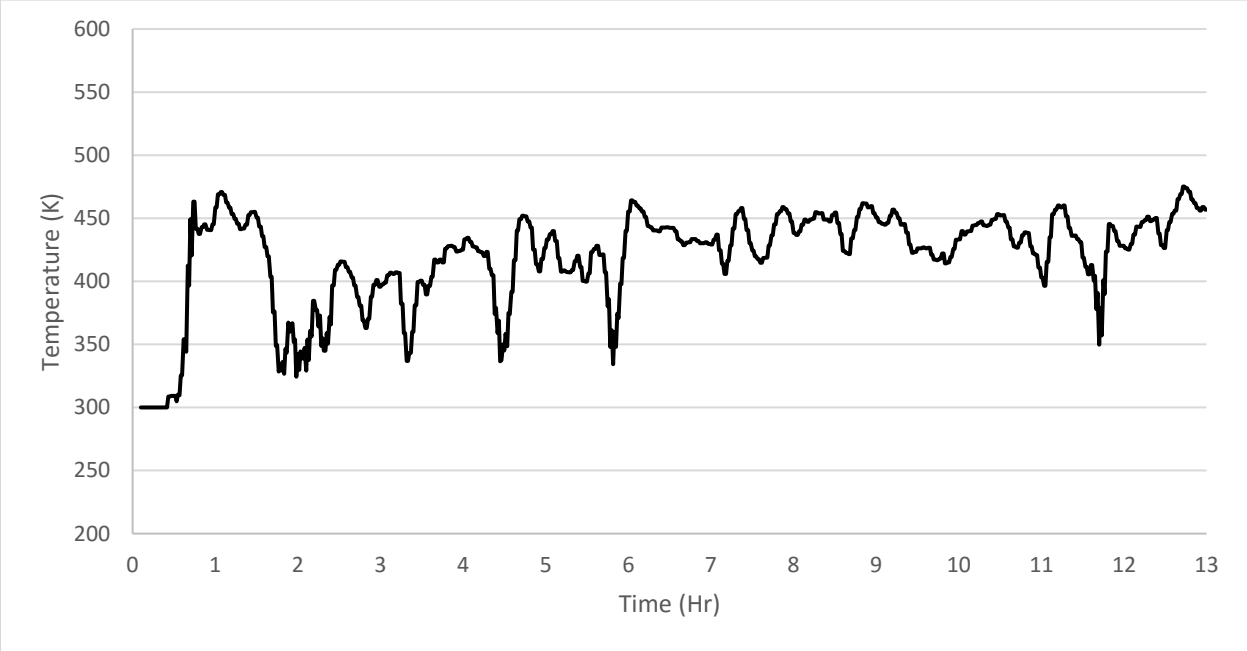

Figure 20. 100 SCCM PID Output

As seen in Figure 19, there are noticeable high frequency fluctuations in the temperature profile. This is cause by the differences between the simulated system and the experimental system.

In the experimental system setup, the reactor consisted of catalysts packed inside a circular steel tube and placed in the middle of a ceramic tube furnace. The gap between the reactor and the heating element caused a delay between applying the heat and the heating of the reactor. Moreover, the PID controller used in the experimental system was connected to a solid state relay to control the status of the furnace circuits; therefore, when the status of the circuits changed, time was needed for the furnace to reach its signaled heating output.

For the simulation, however, heat was applied directly to the wall of the domain, causing no delay between applying the heat and the heating of the reactor. Moreover, unlike in the experimental reactor setup, for the model developed in this dissertation, the domain only consisted of porous media. Because no metal wall was modeled between the heat source and the domain, the heat capacity of the metal wall was not considered. Also, a PID controller was used to directly control the heating in the simulation, resulting in no time delay when transferring the output signal of the PID controller to the heating of the domain wall. These factors caused the thermal resistance between the heating element and the reactor to be greater in the experiment than in the simulation. Therefore, the reactor in the experiment was less sensitive to the change of applied heat in each time step compared to the reactor in the simulation.

Figure 20 shows the output temperature desired by the PID controller. In the beginning, the controller was "learning" the thermal characteristic of the system, and later, the output temperature started to gradually increase, and finally settled at around 450 K.

The fluctuations in the simulation results can be reduced by applying a moving average trend line. The goal for applying the moving average trend line is to reduce the influence of the short term fluctuations and display the long term system behavior with time, therefore, a 20 minute

window size was used for calculating the trend line. With this trend line, it can be used to better compare the system behavior between the simulation results and the experimental data. Figure 21 shows the plot of this trend line from the simulation against the results from the experiment.

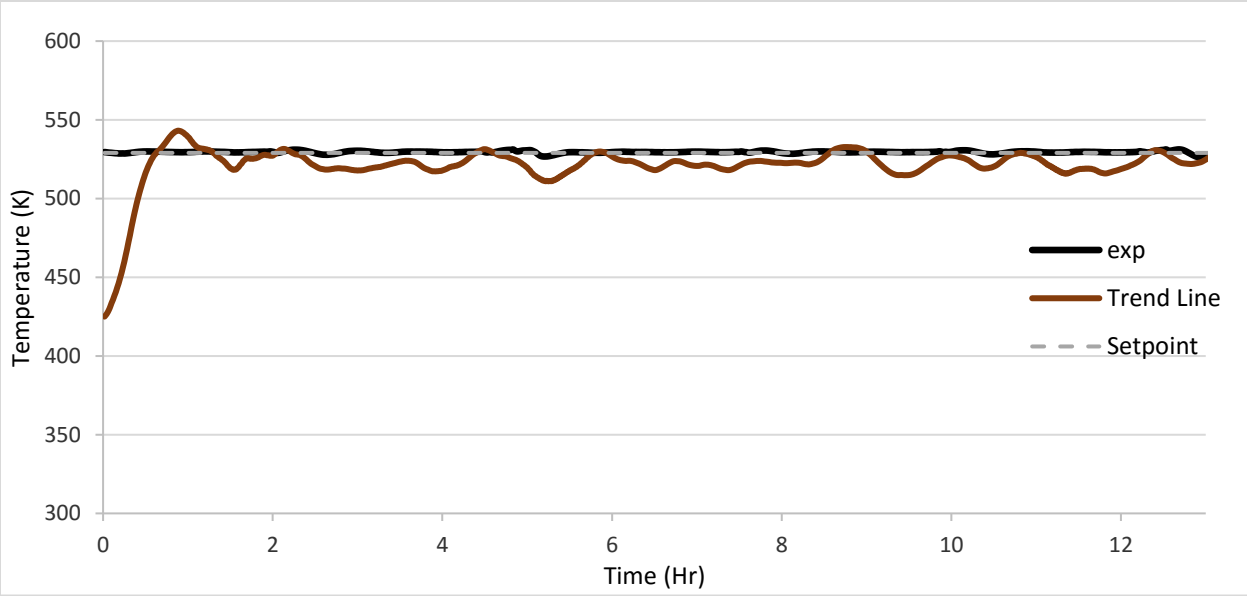

Figure 21. Comparison between Simulation and Experiment for 100 SCCM System

From Figure 21, a similar observation can be made from both the simulation results and the experimental data. In the system with the inlet flow rate of 100 SCCM, the PID controller was able to maintain the system temperature within a 5% error band, and the trend of the simulation results shows a mostly constant system temperature output. This result was expected as the heat energy released from the system was lower than the maximum limit value the PID controller could handle, as shown in Table 13.

Next, a system with a 300 SCCM inlet flow rate was simulated with the PID controller, Figure 22 shows a plot of the simulated system temperature, and Figure 23 shows the PID output temperature for this flow rate.

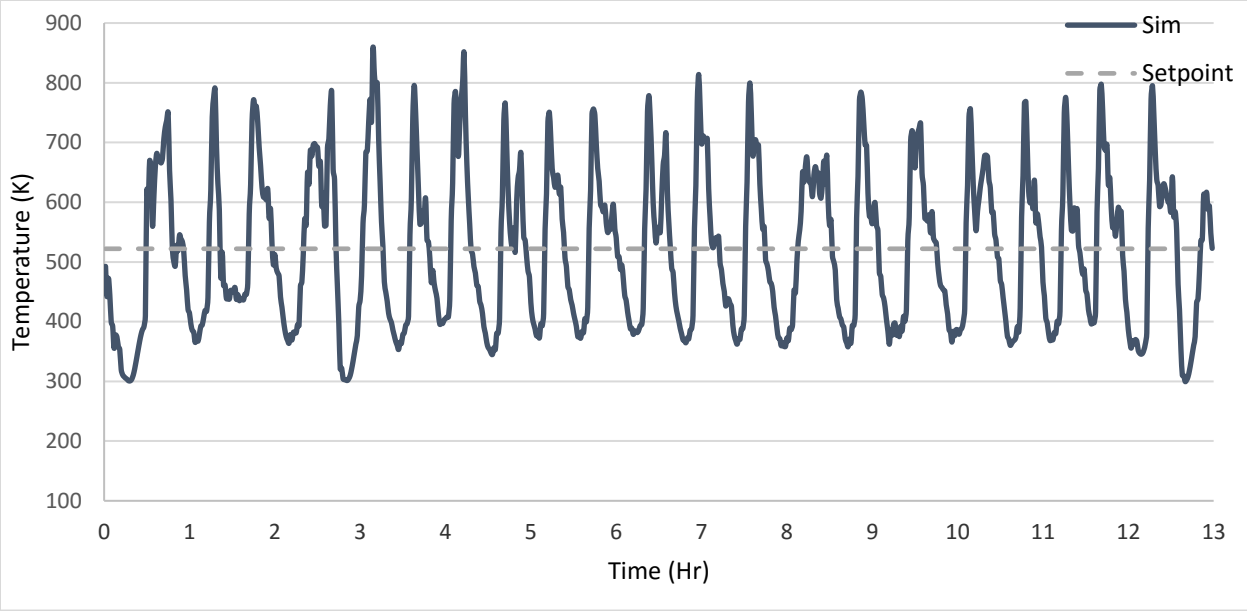

Figure 22. 300 SCCM Simulation Results

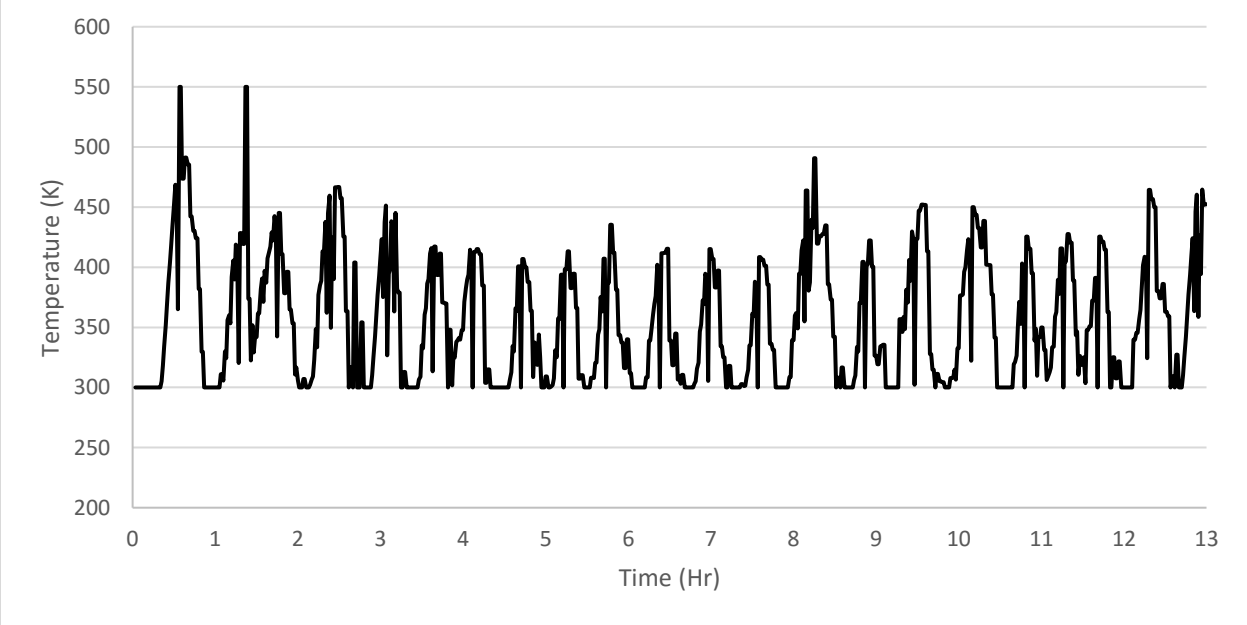

Figure 23. 300SCCM PID Output

As observed from Figure 22, the overshoot was larger compared to the one observed from the experiment with the same flow rate. This is most likely due to the factors mentioned before. Moreover, the amount of heat created in the system was determined by the formation rates of products, and since the expression is an empirical model, therefore, it is data specific. Due to the

lack of experimental data, however, some of the values for those expressions in this dissertation can only be obtained from the literature. Therefore, the values of the system temperature simulated in this case most likely does not closely represent the values obtained from the experiment. Even though the temperature magnitude cannot be accurately captured, the system behavior between the simulation and the experiment should remain close, as long as the reaction mechanism in the system does not change. To better display the system behavior, a moving average trend line was applied to the simulation results and plotted against the experimental data, as shown in Figure 24.

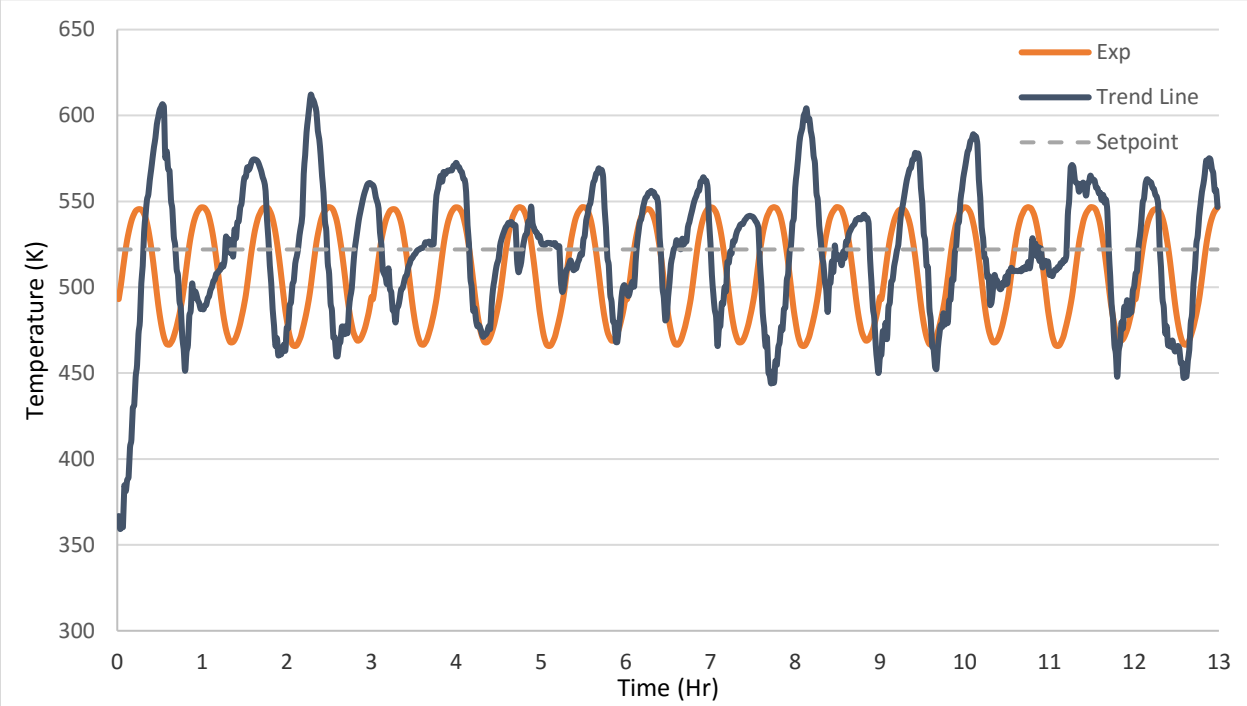

Figure 24. Comparison between Simulation and Experiment for 300 SCCM System

The plot in Figure 24 shows a reasonable agreement between the trend line and the experimental data. The trend line of the results shows that the simulated system have the ability to repeat the experiment with an agreeable result. From observation, starting around 2 hours of simulation time, the sim frequency of the simulation system began to match the frequency obtained from the experiment. Even though the instability of the reaction and the high temperature

sensibility of the reactor had sometimes caused disturbance in the simulation system's frequency and led to a time shift compared with the frequency of the experiment, as observed in Figure 24, this time shift was always able to disappear within 2 cycles.

To further determine how well the simulation results compared to the experimental results, the mean absolute percentage error was calculated. The mean percentage error calculates how well actual values are forecast [70]:

$$MAPE = \frac{100\%}{n}\sum_{t=1}^{n}\left|\frac{a_t - f_t}{a_t}\right| \tag{6.27}$$

Where n is the number of time steps, a_t is the actual value of the quantity, and f_t is the forecast value. Table 14 reports the mean percentage error between the simulation data and the experimental data for both the 100 SCCM and 300 SCCM models,

Table 14. Mean Percentage Error Values

Inlet flow rate [SCCM]	**MPE [%]**
100	2.7
300	24.3

CHAPTER 7

SUMMARY & CONCLUSION

In this dissertation, FTS process experiments were performed with different reactant flow rates, and the system temperature oscillations were observed in the system with high reactant flow rate. It was hypnotized that these temperature oscillations were introduced by the PID controller with unsuitable setting. Since the FTS process itself is an exothermic reaction (ΔH = -146 kJ/mol) [9], as the catalyst becomes more productive, the heat power density increases in the system, causing the difficulty for the controller to maintaining the system at a desired temperature. Attempting to solve this problem by using computational tool available, a multi-platform simulation using FLUENT and MATLAB was proposed to simulate the reaction coupled with PID control method used in the experiment.

In order to demonstrate the viability of the platform, cases study of the different non-linearity for the reaction term was done. The results from the simulation using PID controller supported the hypothesis by showing the similar temperature oscillations in the system. As an increased reactant flow rate was applied to a system, the PID controller had difficulty maintaining the set point because of the increased reaction heat power density. The increase of the reaction power density was a direct result of an increased reaction rate caused by the high reactant flow rate applied to the system. However, the PID method was shown successfully on controlling a system with a lower reaction power density caused by reducing the applied flow rate.

Next, the FTS process simulation reported from the literature was reproduce using FLUENT to validate the simulation setting for this process. The comparison between the reported results and the results obtained in this dissertation was agreeable.

Lastly, the kinetic model of the FTS process was developed with the rate expression obtained from literature and the data obtained from the experiments presented in this dissertation. After the kinetic model specific for this dissertation was developed, it was coupled with the multi-platform simulation system shown earlier to simulate the FTS process. The results from the simulation and the experiment was compared, and showed that the simulation was successful on showing the system temperature behavior display by the experiment.

With the reported simulation performance, it verifies that the feasibility of using such platform to test control algorithm settings before implementing it into the experimental system, in order to reduce the need to do numerous bench-top scale experiments in the laboratory. The benefits of such including reduce the operation costs, increase time efficiency, and reduce the risk of preforming experiments with unknown system behavior.

CHAPTER 8

FUTURE WORK

With this dissertation demonstrated the feasibility of using the multi-platform software system to test the control algorithm before implementing it into the experimental system, many opportunities for improving or extending the scoop of this dissertation remain. There are few directions presented below.

In order to improve the simulation for the experiment, the surrounding space of the reactor should also be considered in the simulation. Instead of applying the controlled heat directly to the reactor's wall as presented in this dissertation, to better represent the thermal resistance showed in the experimental system, the controlled heat should be applied to the reactor's surrounding domain. This process would better simulate the relationship between the controlled heat and the temperature of the reactor.

To improve the FTS kinetic model, more data points on different system temperatures are necessary. To use the non-linear regression algorithms, like the direct search method proposed by Hooke and Jeeves [51], and to obtain all of the unknown variables for the FTS kinetic model, data points from at least four different system temperatures are needed.

The effect of different control algorithms on the FTS process should be investigated. With the use of the multi-platform simulation system developed in this dissertation, the process of investing different control algorisms should be feasible and time efficient.

APPENDIX

A. PID Program

```
%% Input Data

clc; close all; clear all;

Fontsize = 9;

set(0,'defaulttextinterpreter','latex')

set_temp=522; %temperature in K

Kp=2.12;

Ki=0.01;

Kd=86.9;

dt=1.0;

old_time = 0.0;

iteration=2.0;

fprintf('MATLAB program started\n');

%% write inital data to temp.txt

fout = fopen('temp.txt', 'w');

fprintf(fout, '%f', 500.0); % set the initial temperature in K

fclose(fout);

%% write inital error to old_data.txt

fo = fopen('old_data.txt', 'w');

fprintf(fo, '%f %f', 0.0, 0.0);

while exist('dummy.txt','file') == 0   %Fluent is running

%% Wait for signal from Fluent

 while exist('mready.txt','file') == 0

 pause(1);

 end

%% Read in data from Fluent output file

 system('tail -n 1 ./surface1.out > ./surface1.inp');

 fp = fopen('surface1.inp','r');

 t1 = fscanf(fp, '%f');

 time = t1(1);
```

```
surface_temp = t1(2)+awgn(1,1,1);% noise
fclose(fp);
fprintf('MATLAB: Fluent time = %f, Fluent temperature = %f\n', time, surface_temp);
delete('mready.txt');
        while old_time ~= time
%%PID calculation
            if set_temp ~= surface_temp
        fin = fopen('old_data.txt','r');
        t1 = fscanf(fin, '%f');
        old_error = t1(1);
        old_area = t1(2);
        fclose(fin);
                    error=set_temp-surface_temp;
                    P=Kp*error;
                    area=((dt*(error+old_error))/2.0);
        I=Ki*(old_area+area);
                    old_area=old_area+area;
                    D=Kd*(error-old_error)/dt;
                    temp=P+I+D;
                     if temp <= 300
                            temp= 300;
                    end
                    if temp >= 800
                            temp=800;
                    end
                old_error = error;
              %% write data to temp.txt
                    fout = fopen('temp.txt', 'w');
                    fprintf(fout, '%f', temp);
        fclose(fout);
      %% write error to old_data.txt
                    fo = fopen('old_data.txt', 'w');
```

```
                    fprintf(fo, '%f %f', old_error, old_area);
                fclose(fo);
            end
                old_time = time;
        end
 fprintf('MATLAB: current time step = %d\n', iteration);
 iteration=iteration+1.0;
system('touch fready.txt');
%% write data to temp.txt
 fin = fopen('temp_in.dat', 'a');
 fprintf(fin, '%f\n', temp);
 fclose(fin);
%% write data for plotting
 fo = fopen('temp.dat', 'a');
 fprintf(fo, '%f %f\n', time, surface_temp);
 fclose(fo);
end
fprintf('MATLAB: Calculation Completed!\n');
%% Plot result by importing temperature data from dat file
load temp.dat
time_store = temp(:,1);
Temp_store = temp(:,2);
% Time history of temperature variation
figure;
plot(time_store,set_temp*ones(length(time_store)),'k','LineWidth',2)
hold on
plot(time_store,Temp_store,'b*-','LineWidth',2)
xlabel('time (seconds)');
ylabel('Reactor Temperature (K)');
% Time history of temperature variation
load temp_in.dat
time_in = temp_in(:,1);
```

```
figure;
plot(time_store,set_temp*ones(length(time_store)),'k','LineWidth',2)
plot(time_in,'b*-','LineWidth',2)
xlabel('time (seconds)');
ylabel('Fluent Input Temperature (K)');
```

B. UDF Programs

B.1 Wall Temperature

```
#include "udf.h"
#include "unistd.h"

static int last_ts = -1;
float Temp=0;  /* Temp needs to keep same data for multiple calls of this function */
DEFINE_PROFILE(my_temp, thread, position)
{
        face_t f;
        /*char filename[] = "fready.txt";*/
        int curr_ts, time;
        float surface_temp;
        FILE *fp,*fin, *fi, *fo;
        curr_ts = N_TIME;
  /* execute the following lines for a new time step (not sub-iterations) and not initial time step */
   if(curr_ts>1 && curr_ts != last_ts){
      Message("Fluent: Time step = %d\n",curr_ts);
      last_ts=curr_ts;
       /*update temp.txt*/
        system("tail -n 1 ./surface1.out > ./surface1.inp");
            fp = fopen("surface1.inp","r");
            fscanf(fp, "%d %f", &time, &surface_temp);
        fclose(fp);
```

```
            fo = fopen("temp.txt","w");
            fprintf(fo, "%f", surface_temp);
            fclose(fo);
      /* monitor data is only available after the first time step has been completed */
      /*signal Matlab that Fluent output data from previous iteration is
        available to read */
      /* system("touch mready.txt");*/
        fi = fopen("mready.txt","w");
        fclose(fi);
/*wait for Matlab signal that boundary data is available to read*/
            fp=NULL;
            while (fp == NULL){
       system("sleep 1");
             fp = fopen("fready.txt","r");
            }
     Message("FLUENT: fready.txt found, time = %d\n",curr_ts);
     fclose(fp);
            /* read temperature from MATLAB */
            fin = fopen("temp.txt", "r");
            fscanf(fin, "%f", &Temp);
            fclose(fin);
     /* remove signal file */
            remove ("fready.txt");
  }
  else if( curr_ts==0 || curr_ts==1)
    Temp=500;   /* initialize with this temperature, use this for 1st time step */
    /* apply boundary condition */
  Message("Fluent: Applying temperature = %f at time step = %d\n",Temp,curr_ts);
  begin_f_loop(f,thread){
    F_PROFILE(f,thread,position)=Temp;
  }
```

```
    end_f_loop(f,thread)
}
```

B.2 Diffusion

```
#include "udf.h"

int count = 0;

DEFINE_DIFFUSIVITY(diffusion,c,t,i)

{

Domain *d;

Material *m,*sp;

div_t divide;

int j1,j2,k,n,ns,nspe,flag;

real diff, d_m[20][20];

real T;

T = C_T(c,t);

d_m[0][1] = 1.25e-10*pow(T,1.75);

d_m[0][2] = 2.27e-11*pow(T,1.75);

d_m[0][3] = 9.63e-11*pow(T,1.75);

d_m[0][4] = 1.68e-11*pow(T,1.75);

d_m[0][5] = 3.8e-10*pow(T,1.75);

d_m[1][2] = 3.22e-11*pow(T,1.75);

d_m[1][3] = 1.36e-10*pow(T,1.75);

d_m[1][4] = 2.35e-11*pow(T,1.75);

d_m[1][5] = 5.45e-10*pow(T,1.75);

d_m[2][3] = 2.86e-11*pow(T,1.75);

d_m[2][4] = 4.14e-12*pow(T,1.75);

d_m[2][5] = 1.05e-10*pow(T,1.75);

d_m[3][4] = 2.14e-11*pow(T,1.75);

d_m[3][5] = 3.73e-10*pow(T,1.75);

d_m[4][5] = 7.69e-11*pow(T,1.75);

m=THREAD_MATERIAL(t);

n=MIXTURE_NSPECIES(m); /*n->no. of species, n-1 no of eqns*/

flag = 0;
```

```
k=n-1;


/*Get j1 and j2 from i from the formulae i=j1*(no of species-1)+j2-1 and j1<j2*/

/*then use j1 and j2 to specify binary diffusivity d(j1,j2)*/

while (flag==0)

{

divide=div((i+1-k),(n-1));

if(divide.rem==0.0)

{ j2=k;

flag=1;}

else

k=k-1;

}

j1=(i+1-j2)/(n-1);

diff= d_m[j1][j2];

/*Message("i: %d diff:%g d_m[%d][%d] \n",i,diff,j1,j2);*/

return diff;

}
```

B.3 Reaction Rate

```
#include "udf.h"

 #include "math.h"

   DEFINE_VR_RATE(rx_rate,c,t,r,mole_weight,species_mf,rate,rr_t)

 {

  real T, P, rho ;

  real m, r_ft;

  real m_CO, m_H2O, m_C14H30, m_CH4, m_C25H52, m_H2;

  real mole_fraction_CO, mole_fraction_H2;

  real p_CO, p_H2;

  /*Fluent solves for the mass fraction of the species. Convert this to mole fraction, which is directly proportional to the partial pressure.*/

  T = C_T(c, t);

  P = C_P(c,t)*9.87e-6;  /*change unit from Pa to atm*/
```

```
  rho = C_R(c,t);
  m_CO = species_mf[0]/mole_weight[0]; /*mole_weight[i];  number of mole = mass fraction / mole weight*/
  m_H2O = species_mf[1]/mole_weight[1];
  m_C14H30 = species_mf[2]/mole_weight[2];
  m_CH4 = species_mf[3]/mole_weight[3];
  m_C25H52 = species_mf[4]/mole_weight[4];
  m_H2 = species_mf[5]/mole_weight[5];
  m = m_CO + m_H2O + m_C14H30 + m_CH4 + m_C25H52 + m_H2; /*total mole weight*/
  mole_fraction_CO = m_CO/m;
  mole_fraction_H2 = m_H2/m;
p_CO = mole_fraction_CO*P;  /* partial pressure */
  p_H2 = mole_fraction_H2*P;
   /*If more than one reaction is defined, it is necessary to distinguish
     between these using the names of the reactions.     */
   if (!strcmp(r->name, "reaction-1"))
      {
        /* Reaction 1 */
           r_ft=(3.42*exp(-100000 / (8.314 * T))*(40.1*species_mf[0])*(40.6*species_mf[5]))/(pow(1+0.45*exp(-20000 / (8.314
* T))*(40.1*species_mf[0]),2)); /*mol/g-s*/
             *rate = 1.94*exp(-81000 / (8.314 * T))*r_ft*rho;
          if (T >= 550)
          {
            *rate = 0;
                }
         if (T <= 450)
          {
            *rate = 0;
                }
              if (p_CO == 0)
          {
            *rate = 0;
                }
```

```
    }
 else if (!strcmp(r->name, "reaction-2"))
       {
       /* Reaction 2 */
        *rate = pow(-0.0106*T+6.5796,14) * (0.0424*T-22.24)* -((1.64e5*exp(-105000/(8.314*T)))*pow(p_CO,-0.5)*pow(p_H2,0.68))*rho;  /*mol/g-s*/
          if (*rate < 0)
           {
             *rate = 0 ;
           }
          if (p_CO == 0)
           {
             *rate = 0;
                 }
          if (p_H2 == 0)
           {
             *rate = 0;
                 }
          if (T >= 550)
            {
             *rate = 0;
                  }
          if (T <= 450)
            {
             *rate = 0;
                 }
       }
     else if (!strcmp(r->name, "reaction-3"))
       {
          /* Reaction 3 */
```

```
        *rate = pow(-0.0106*T+6.5796,25) * (0.0058*T-3.0769) * -(1.64e5*exp(-105000/(8.314*T))*pow(p_CO,-0.5)*pow(p_H2,0.68))*rho;  /*mol/g-s*/

            if (*rate < 0)

       {

         *rate = 0;

       }

      if (p_CO == 0)

       {

         *rate = 0;

            }

          if (p_H2 == 0)

       {

         *rate = 0;

            }

      if (T >= 550)

       {

         *rate = 0;

            }

       if (T <= 450)

       {

         *rate = 0;

            }

  }


else

  {

    Message("Unknown Reaction\n");

  }
```

```
}
```

B.4 Flow Rate

```
#include "udf.h"

DEFINE_PROFILE(FR,t,i)

{

real x[ND_ND]; /* this will hold the position vector */

real xcor,ycor;

real T, P ;

face_t f;

cell_t c;

begin_f_loop(f,t)

{

 F_CENTROID(x,f,t);

  xcor=x[1];

 ycor = x[2];

 T = C_T(c, t);

 P = C_P(c,t);


 F_PROFILE(f,t,i) = (0.032)*(P/(8.314*T))*(0.018/3600); /* density = Wn_syn[kg]*(P[Pa]/R*T) */

}

end_f_loop(f,t)

}
```

C. Lump mass model derivation

From the first law of thermodynamics,

$$\frac{dE}{dt} = \dot{Q} \tag{B1}$$

where E is the energy, and $\dot{Q}$ is rate of heat transfer to the system.

For a control volume, the above equation can be express as,

(change of energy in CV) =

(heat added to CV) + (energy flow into CV) - (energy flow out of CV) (B2)

Where CV is control volume.

$$\text{change of energy in CV} = \frac{\partial}{\partial t}\int \rho e dV \tag{B3}$$

where ρ is density and e is the internal energy.

For prefect gas,

$$e = CpT \tag{B4}$$

Where Cp is the heat capacity and T is the temperature.

Therefore, with definition of (C4), equation (C3) become

$$\text{change of energy in CV} = \frac{\partial}{\partial t}\int \rho CpT dV \tag{B5}$$

For a 0-D lump mass, equation (C5) become,

$$\frac{\partial}{\partial t}\int \rho CpT dV = \rho C_p V\dot{T} \tag{B6}$$

Heat added to the system due to conduction and reaction is considered, so for the 0-D lump mass model,

$$\text{heat added to CV} = -k\frac{T_{wall}-T_{meas}}{l}SA + AT^nV \tag{B7}$$

and energy flow of the CV is,

$$(\text{energy flow into CV}) - (\text{energy flow out of CV}) = \dot{m}C_pT_{in} - \dot{m}C_pT_{out} \tag{B8}$$

Therefore, for the rate of temperature change for the CV is,

$$\dot{T} = \frac{1}{\rho C_p V}\left[\dot{m}C_p(T_{in} - T_{out}) + AT^nV - k\frac{T_{wall}-T_{meas}}{l}SA\right] \tag{B9}$$

REFERENCE

[1] The World Factbook, Washington: DC: Central Intelligence Agency, 2013-14.

[2] "Benefits and use of natural gas," [Online]. Available: http://www.encana.com/natural-gas.natural-gas-101/benefits.html.

[3] S. Shahhosseini, S. Alinia and M. Irani, "CFD simulation of fixed bed reactor in Fischer-Tropsch Synthesis of GTL technology," *International Journal of Chemical, Molecular, Nuclear, Materials and Metallurgical Engineering,* vol. 3, no. 12, 2009.

[4] P. Sabatier and J. Sederens, "New mehtane synthesis," *Academy of Sciences,* vol. 134, p. 514, 1902.

[5] BASF.German 1913.

[6] F. Fischer and H. Tropsch, "Preparation of synthetic oil mixtures (Synthol) from Carbon Monoxide and Hydrogen," *Brennstoff-Chemie,* vol. 4, pp. 276-285, 1923.

[7] J. Casci, C. Lok, and M. Shannon, "Fischer-Tropsch catalysis: The basis for an emerging industry with origins in the early 20th century," *Catalysis Today,* vol. 145, p. 38, 2009.

[8] R. Anderson, Catalysis, New Jersey: Van Nostrand-Reinhold, 1956.

[9] M. Dlamini, Literature review: Fischer-Tropsch synthesis, 2012.

[10] M. Dry, "The Sasol route to chemical and fuels," *Studies in Surface Science and Catalysis,* vol. 36, pp. 447-456, 1988.

[11] A. Miroliaei, F. Shahraki, H. Atashi and R. Karimza, "Comparison of CFD results and experimental data in a fixed bed Fischer-Tropsch Synthesis reactor," *Journal of Industrial and Engineering Chemistry,* pp. 1912-1920, 2012.

[12] M. Dry, "Fischer-Tropsch Sythesis - Industrial," in *Encyclopedia of Catalysis*, John Wiley & Sons, Inc, 2010.

[13] H. Schlz, B. Rao and M. Elstner, *Erdol und Kohle,* vol. 22, p. 651, 1970.

[14] A. Steynberg and M. Dry, Fischer-Tropsch Technology, Elsevier, 2004.

[15] A. Anderson and S. Choe, "Ethglene hydrogenation mechanism on the platinum (111) surface: Theoretical determination," *The Journal of Physical Chemistry B,* vol. 93, p. 6145, 1989.

[16] S. Sie, "Process development and scale up: IV. Case history of the development of Fischer-Tropsch synthesis process," *Reviews in Chemical Engineering,* no. 14, pp. 109-137.

[17] G. Blyholder, "Molecular orbital view of chemisorbed Carbon Monoxide," *The Journal of Physical Chemistry,* vol. 68, p. 2772, 1964.

[18] U. Roland, U. Braunschweig and F. Roessner, "On the nature of split over hydrogen," *Journal of Molecular Catalysis A: Chemical,* vol. 127, p. 61, 1997.

[19] B. Hammer, Y. Morikawa and J. Norskov, "CO chemisorption of metal surface and over layers," *Physical Review Letter,* vol. 76, p. 2141, 1996.

[20] Q. Ge, M. Neurock, H. Wright and N. Srivinas, "A first principles of study of carbon-carbon coupling over the {0001} surface of Co and Ru," *The Journal of Physical Chemistry B,* vol. 106, p. 2826, 2002.

[21] D. Do, H. Do and D. Nicholson, "A computer appraisal of BET theory, BET surface area and the calculation of surface excess for gas adsorption on a graphite surface," *Chemical Engineering Science,* vol. 65, no. 10, pp. 3331-3340, 2010.

[22] P. Munnik, P. de Jongh and K. de Jong, "Control and impact of the nanoscale distribution of supported Cobalt particles used in Fischer-Tropsch catalysis," *Journal of American Chemical Society,* vol. 136, no. 20, pp. 7333-7340, 2014.

[23] G. Arzamendi, P. Dieguez, M. Montes and J. Odrioz, "Computational Fluid Dynamics study of heat transfer in microchannel reactor for low-temperature Fischer-Tropsch Synthesis," *Chemical Engineering Journal,* vol. 160, pp. 915-922, 2012.

[24] Y. Liu, Z. Zhang and S. Xiao, "Preparation and properties of cobalt oxides coated carbon fibers as microwave-absorbing materials," *Applied Surface Science,* vol. 257, no. 17, pp. 7678-7683, 2011.

[25] C. Bianchi, C. Pirola and V. Ragaini, "Choosing the best diluent for a fixed catalytic bed: The case of CO hydrogenation," *Catalysis Communications,* vol. 7, no. 9, pp. 669-672, 2006.

[26] Y. Wang, Y. Xu, Y. Li and Y. Long , "Heterogeneous modeling of fixed-bed Fischer-Tropsch synthesis: Reactor model and its applications," *Chemical Engineering Science,* vol. 58, pp. 867-875, 2003.

[27] M. Irani, A. Alizadehdakhel, A. Pour and O. Proulx, "An investigation on the oreformance of a FTS fixed-bed reactor using CFD methods," *International Communications in Heat and Mass Transfer,* vol. 38, pp. 1119-1124, 2011.

[28] S. Rodani, D. Quail and N. Bakhshi, "Self-turning control of Fischer-Tropsch synthesis in a Tube-wall reactor," *The Canadian Journal of Chemical Engineering,* vol. 66, pp. 485-492, 1988.

[29] A. Arpornwichanop, P. Kittisupakorn and M. Hussain, "Model-based control strategies for a chemical reactor with exothermic reactions," *Korean Journal of Chemical Engineering,* vol. 19, no. 2, pp. 221-226, 2002.

[30] C. Karr, S. Sharma, W. Hatcher and T. Harper, "Fuzzy control of an exothermic chemical reaction using Genetic Algorithms," *Engineering Application of Artificial Intelligence,* vol. 6, no. 6, pp. 575-582, 1993.

[31] C. Pinheiro and L. Kershenbaum, "Model predictive control of reactor temperature ina CSTR pilot plant operating at an unstable steady-state," *Computer and Chemical Engineering Supplement,* 1999.

[32] P. Afonso, N. Oliveira and J. Castro, "Model predictive control of a pilot plant reactor with a simulated exothermic reaction," *Computer Chemical Engineering,* vol. 20, pp. 769-774, 1996.

[33] S. Pennycook, A. Lupini, A. Borisevich and M. Var, Transmission Electron Microscopy: Overview and Challenges.

[34] I. Currie, Fundamental Mechanics of Fluids, New York: CRC Press, 1993.

[35] J. Anderson, Computational Fluid Dynamics: The Basic with Application, New York: McGraw-Hill, Inc..

[36] W. Krantz, Scaling Analysis in Modeling Transport and Reaction Processes: A Systematic Approach to Model Building and the Art of Approximation, A John Wiley & Sons, INC., 2007.

[37] F. Haugen, PID Control, Trondheim: Tapir Academic Press, 2014.

[38] J. Ziegler and N. Nichols, "Optimum setting for automatic controllers," *ASME,* vol. 64, pp. 759-768, 1942.

[39] E. Mokheimer, M. Hussain, S. Ahmed, M. Habib and A. Ai-Qutub, "On the modeling of steam methane reforming," *Journal of Energy Resource Technology,* vol. 137, 2015.

[40] R. Holdich, "Fluid flow in porous media," in *Fundamentals of Particle Technology*, Midland Information Technology & Publishing, 2002.

[41] "Rock Porosity," NED University of Engineering and Technology, 2016.

[42] G. Batchelor, An Introduction to Fluid Dynamics, Cambridge: Cambridge Univ. Press, 1967.

[43] "ANSYS FLUENT 12.0 User's Guide," Ansys Inc., 2009.

[44] T. Radoičić, M. Đuriš, R. Garić-Grulović, Z. Arsenijević and Z. Grbavčić, "Particle characterization of polydisperse quartz filtration sand," *Powder Technology,* vol. 254, pp. 63-71, 2014.

[45] W. Wilcox, *Definition and calculation of sphericity of particles,* Clarkson University, 2009.

[46] K. Sutton and P. Gnoffo, "Multi-component diffusion with application to computational aerothermodynamics," in *7th AIAA/ASME Joint Thermophysics*, Albuquerque, 1998.

[47] R. Reid, J. Prausnitz and B. Poling, The Properties of Gases and Liquids, New York: Mc-Graw-Hill, 1987.

[48] R. Bird, W. Stewart and E. Lightfoot, Transport Phenomena, New York: John Wiley & Sons, 2002.

[49] S. Choi, A. Rege and B. Dennis, "Simulation platform for rapid testing of methods to control exothermic chemical reactions," in *International Mechanical Engineering Congress and Exposition*, Hou, 2015.

[50] J. Simmie, "Detailed chemical kinetic models for the combustion of hydrocarbon fuels," *Progress in Energy and Combustion Science,* vol. 29, no. 6, pp. 599-634, 2003.

[51] R. Everson, H. Mulder and M. Keyser, "The Fischer-Tropsch reaction with supported ruthenium catalysis: Modelling and evaluation of the reaction rate equation for a fixed bed reactor," *Applied Catalysis A: General ,* vol. 142, pp. 223-241, 1996.

[52] G. Thompson, A. Vickers and P. Pujado, "Mathematically modeled comparison of Fischer-Tropsch reactor systems," UOP Process Division, Illinois.

[53] W. Zimmerman, *Kinetic modeling of the Fischer-Tropsch Sythesis,* College Station: Texas A&M University, 1990.

[54] A. Sharma, R. Philippe, F. Luck and D. Schweich, "A simple and realistic fixed bed model for investigating Fischer-Tropsch catalyst activity at lab-scale and extrapolating to industrial conditions," *Chemical Engineering Science,* vol. 66, pp. 6358-6366, 2011.

[55] D. Bates and D. Watts, Nonlinear Regression Analysis and Its Applications, Hoboken: John Wiley & Sons, Inc., 1988.

[56] G. Froment, "The kinetics of complex catalytic reactions," *Chemical Engineering Science,* vol. 42, no. 5, pp. 1073-1087, 1987.

[57] R. Anderson, F. Karn and J. Shultz, "Kinetics of the Fischer-Tropsch Synthesis on iron catalysts," Van Nostrand-Reinhold, New York, 1956.

[58] H. Atwood and C. Bennett, "Kinetics of the Fischer-Tropsch Reaction over Iron," *Industrial & Engineering Chemistry,* vol. 18, no. 1, pp. 163-170, 1979.

[59] G. Huff and C. Satterfield, "Evidence for two chain growth probabilities on iron catalysts in the Fischer-Tropsch synthesis," *Journal of Catalysis,* vol. 85, no. 2, pp. 370-379, 1984.

[60] R. Philippe, M. Lacroix, L. Dreibine, C. Pham-Huu, D. Edouard, S. Savin, F. Luck and D. Schweich, "Effect of structure and thermal properties of a Fischer–Tropsch catalyst in," *Catalysis Today,* vol. 147, pp. 305-312, 2009.

[61] G. P. Laan, "Kinetics, Selectivity and Scale Up of the Fischer-Tropsch Synthesis," University of Groningen, Netherlands, 1999.

[62] A. Zein El Deen, J. Jacobs and M. Baerns, "Kinetic Measurements of the Hydrogenation of Carbon Monoxide (Fischer-Tropsch Synthesis) Using an Internal Recycle Reactor," *ACS Symposium Series,* vol. 65, pp. 26-36, 1978.

[63] G. Bub and M. Baerns, "Prediction of the performance of catalytic fixed bed reactors for Fischer-Tropsch Synthesis," *Chemical Engineering Science,* vol. 35, no. 1-2, pp. 348-355, 1980.

[64] C. Kellner and A. Bell, "The kinetics and mechanism of carbon monoxide hydrogenation over Alumina_supported Ruthenium," *Journal of Catalysis,* 1980.

[65] D. Himmelblau, Process Analysis by Statistical Methods, New York: John Wiley, 1970.

[66] A. Tavakoli, M. Sohrabi and A. Kargari, "Application of Anderson-Schulz-Flory (ASF) equation in the product distribution of slurry phase FT synthesis with nanosized iron catalysts," *Chemical Engineering Journal,* vol. 136, pp. 358-363, 2008.

[67] J. Wang, "Physical, chemical, and catalytic properties of boried cobalt Fischer-Tropsch catalysts," Brigham Young University, 1987.

[68] E. Fuller, P. Schettler and J. Giddings, "A new method for prediction of binary gas-phase diffusion coefficients," *Industrial and Engineering Chemistry,* vol. 58, no. 5, pp. 19-27, 1966.

[69] "How Do I Convert PID Parameters From Gain to Time?," National Instruments, 28 4 2014. [Online]. Available: http://digital.ni.com/public.nsf/allkb/6E76EC47B831FAED86256E4E007347DC. [Accessed 15 7 2016].

[70] S. Kim and H. Kim, "A new metric of absolute percentage error for intermittent demand forecasts," *International Journal of Forecasting,* vol. 32, no. 3, pp. 669-679, 2016.

[71] S. Qi and T. Badgwell, "A survey in industrial model oredictive control technology," *Control Enrgineering Practice,* vol. 11, pp. 733-764, 2003.

[72] A. McIntosh, S. Shah and D. Fisher, "Analysis and turming of adaptivr generalized predictive control," *The Canadian Journal of Chemical Engineering,* vol. 69, no. 1, pp. 97-110, 1991.

[73] M. Dry, "Practical and theoretical aspects of the catalytic Fischer-Tropsch process," *Applied Catalysis A: General,* vol. 138, no. 2, pp. 319-344, 1996.

[74] M. Cannon, *C21 Model Predictive Control,* Oxford: University of Oxford.

[75] M. Carr, "Computer flow dynamic analysis of 5-hole catalyst geometries in methane stream reforming," Worcester Polytechnic Institute, 2012.

[76] T. Turner, *Modeling and simulation of reaction kinectics for biodiesel production,* Raleigh: North Carolina State University, 2005.

Biographical Information

Siusan Choi received her Bachelor Degrees in both Mechanical and Aerospace Engineering from University of Texas at Arlington in 2010. She started to pursue her PhD degree in Aerospace Engineering at the University of Texas at Arlington right after she received her Bachelor Degrees. Her research mainly focuses on computer simulation study and system control for sustainable energy development. And her research area involves Fisch-Tropsch synthesis and coal pyrolysis.